Combined In Vitro-In Silico Approach to Predict Deposition and Pharmacokinetics of Budesonide Dry Powder Inhalers

Conor A. Ruzycki*, Brynn Murphy, Hafeez Nathoo, Warren H. Finlay, Andrew R. Martin†

Department of Mechanical Engineering, University of Alberta, Edmonton, AB, Canada

* Contact / Submitting Author

† Corresponding Author

Running Head: *In Vitro – In Silico* DPI Characterization

Abstract

Purpose

A combined *in vitro – in silico* methodology was designed to estimate pharmacokinetics of budesonide delivered via dry powder inhaler.

Methods

Particle size distributions from three budesonide DPIs, measured with a Next Generation Impactor and Alberta Idealized Throat, were input into a lung deposition model to predict regional deposition. Subsequent systemic exposure was estimated using a pharmacokinetic model that incorporated Nernst-Brunner dissolution in the conducting airways to predict the net influence of dissolution, mucociliary clearance, and absorption.

Results

DPIs demonstrated significant *in vitro* differences in deposition, resulting in large differences in simulated regional deposition in the central conducting airways and the alveolar region. Similar but low deposition in the small conducting airways was observed with each DPI. Pharmacokinetic predictions showed good agreement with *in vivo* data from the literature. Peak systemic concentration was tied primarily to the alveolar dose, while the area under the curve was more dependent on the total lung dose. Tracheobronchial deposition was poorly correlated with pharmacokinetic data.

Conclusions

Combination of realistic *in vitro* experiments, lung deposition modeling, and pharmacokinetic modeling was shown to provide reasonable estimation of *in vivo* systemic exposure from DPIs. Such combined approaches are useful in the development of orally inhaled drug products.

Keywords (X5)

Budesonide dry powder inhalers

Pharmacokinetics

In vitro in vivo correlations

Bioequivalence

Lung Deposition Modeling

Abbreviations

DPI – dry powder inhaler

NGI – Next Generation Impactor

MMAD – mass median aerodynamic diameter

List of Symbols

ρ_{P}	Particle density
AUC_{24}	Area under the curve (24 hours)
c	Drug concentration
c_{i}	Drug concentration in i$^{\mathrm{th}}$ airway compartment
$c_{\max}$	Maximum serum concentration in central compartment
c_{s}	Drug solubility
CL	Clearance
D	Diffusion coefficient
$d_{\mathrm{g},50}$	Particle geometric mean diameter
F_{BA}	Oral bioavailability
F_{i}	Fraction of dose depositing in i$^{\mathrm{th}}$ compartment
h	Diffusion layer thickness
k_{12}	Central to peripheral rate constant
k_{21}	Peripheral to central rate constant

k_{10}	Elimination rate constant
k_{a}	Oral absorption rate constant
k_{ALV}	Alveolar region absorption rate constant
$k_{\mathrm{diss,ALV}}$	Dissolution rate constant in alveolar region
$k_{\mathrm{muc,i}}$	Mucociliary rate constant for i$^{\mathrm{th}}$ airway compartment
k_{TB}	Tracheobronchial region absorption rate constant
$K_{\mathrm{diss,TB}}$	Effective dissolution rate in tracheobronchial region
m	Drug mass
$m_{i,1}$	Drug mass (solid) in i$^{\mathrm{th}}$ airway compartment
$m_{i,2}$	Drug mass (dissolved) in i$^{\mathrm{th}}$ airway compartment
P_{m}	Measured Pressure
P_{ref}	Reference Pressure
Q	Flowrate
Q_{peak}	Peak inhalation flowrate
R	Inhaler resistance
S	Surface area of particles undergoing dissolution
t	Time
t_{max}	Time at which maximum serum concentration occurs
t_{total}	Duration of inhalation
T_{m}	Measured Temperature
T_{ref}	Reference Temperature
$V_{\mathrm{ASL,i}}$	Volume of airway surface liquid in i$^{\mathrm{th}}$ airway compartment
V_{C}	Volume of central compartment
$V_{\mathrm{d,ss}}$	Volume of distribution at steady state

Subscripts

A	gastrointestinal tract compartment
ALV	alveolar
ASL	airway surface liquid
DPI	at the inlet of the inhaler
DPI exit	immediately downstream of inhaler mouthpiece
HBM	breathing machine line

P	peripheral compartment
TB	tracheobronchial
X	central compartment
supply	building air supply line
std	standard flowrate
vacuum	vacuum line
vol	volumetric flowrate

Introduction

The unique structure and physiology of the respiratory tract make it an attractive route for the delivery of therapeutics. Pharmaceutical aerosols, including bronchodilators and anti-inflammatories, are a mainstay in the treatment of lung disease (1–3), with aerosols providing a vehicle for the direct delivery of therapeutics to the site of intended action. Such targeted delivery generally reduces systemic dosing and associated adverse side effects. Paradoxically, the respiratory tract is also a useful route for the systemic delivery of some medications, as the massive surface area of the gas-exchange region of the lungs can facilitate rapid uptake. Examples of inhalable therapeutics for systemic circulation include insulin for diabetes (4), loxapine for schizophrenia (5), and levodopa for Parkinson's disease (6). Delivery via the inhalation route generally allows for safe and convenient self-administration by patients while bypassing first-pass metabolism.

Dosing of inhaled pharmaceutical aerosols to the lungs, however, is highly specific to individual device-formulation combinations, with considerable inter- and intra-subject variability (7). The physics governing aerosol generation and transport are complex, making it difficult to estimate where particles will deposit in the respiratory tract based on their diameter alone (8). Post-deposition, natural defense mechanisms in the respiratory tract including mucociliary clearance, enzymatic reactions, and resident macrophages all can influence drug localization, metabolism,

absorption and retention (9,10). These considerations highlight the importance of establishing accurate measures of device and formulation performance that enable prediction of delivered doses, and ultimately clinical efficacy.

In vitro experiments, *in silico* computational models, and *in vivo* studies of lung deposition and pharmacokinetics all provide useful data that can inform inhalation device and formulation design (7,11,12). By combining *in vitro* and *in silico* methods, *in vitro* data describing delivered drug mass and particle size distribution serves as input to numerical models that predict lung deposition and pharmacokinetics. Within such an approach, realistic *in vitro* methods can be used to characterize extrathoracic deposition and the initial lung dose, as well as the intra-thoracic particle size distribution (13,14), after which numerical modeling can elucidate information on thoracic deposition and disposition. Several groups have proposed *in silico* models relating regional deposition to systemic exposure or response (15–20) following the initial forays into this approach in the 1980s by Byron (21) and Gonda (22).

In the present work, we demonstrate a method for evaluating dry powder inhaler performance in terms of clinically relevant metrics using a combination of realistic *in vitro* experimentation and *in silico* numerical modeling of lung deposition, airway surface liquid, and pharmacokinetics. Three commercially available budesonide inhalers were selected for comparative study. In an earlier work (14), we evaluated the influences of inhaler insertion angle on deposition from these same DPIs in the Alberta Idealized Throat (providing an *in vitro* measure of extrathoracic deposition), and a downstream filter (providing an *in vitro* measure of the total lung dose). In the present work, we extend that testing to measure the intrathoracic particle size distribution from each DPI, and in conjunction with deposition and disposition modeling, estimate regional lung deposition and the systemic concentration of budesonide achieved with each DPI under typical

use. We extend existing pharmacokinetic models for inhaled corticosteroids, which broadly differentiate lung doses in terms of central and peripheral compartments (15,20,23), to consider the competing mechanisms of particle dissolution, absorption, and mucociliary clearance in each tracheobronchial airway generation. The methods exemplified in the present study are intended to help bridge the gap between *in vitro* benchtop development and early-stage human trials, wherein emphasis is often placed on the systemic dose, particularly during the development and testing of generics (24,25).

Materials and Methods

Three commercially available DPIs with formulation strengths of 200 µg budesonide per dose were selected for testing, including Pulmicort® Turbuhaler® (Lot PASY; AstraZeneca Canada Inc. Mississauga, Canada), Easyhaler® Budesonide (Lot 1820769 Orion Pharma Espoo, Finland), and Budelin® Novolizer® (Lot 7A104; Meda Pharmaceuticals Inc. Takeley, United Kingdom). DPIs were chosen to span a representative range of device resistances expected of typical devices. General characteristics of each DPI are presented in Table 1.

Table 1: Characteristics of each DPI selected for testing, along with inhalation parameters defined using the relations of Delvadia et al (26).

Inhaler	Label Claim (µg budesonide)	Doses	Device Resistance (26) R ($kPa^{1/2}$min/l)	Peak Inhalation Flowrate Q_{peak} (l/min)	Duration of Inhalation t_{total} (sec)
Pulmicort® Turbuhaler®	200	200	0.0352	72.7	3.50
Easyhaler® Budesonide	200	200	0.0435	62.8	4.05
Budelin® Novolizer®	200	100	0.0241	96.5	2.64

A three-part analysis incorporating experimental and numerical methods was developed and employed to compare the performance of these three DPIs having identical label claims. First, DPIs were characterized *in vitro* using measurements in an Alberta Idealized Throat placed upstream of a Next Generation Impactor with pre-separator (Model 170 NGI and pre-separator; MSP Corporation, Shoreview, MN). Second, *in vitro* results were fed into a regional lung deposition model to provide estimates of the initial doses of budesonide depositing throughout the lungs. Third, generational deposition and airway surface liquid concentrations calculated by the lung deposition model were used as input to a pharmacokinetic model to estimate the systemic plasma concentration of budesonide over time in a typical adult human. Specifics of each part of this study are discussed in the following sections.

In Vitro Performance Characterization

Experimental Design

The DPIs selected for the present study are passive devices, with each exhibiting some degree of flowrate-dependent performance (27). With each DPI having a different airflow resistance, a subject inhaling with a certain inspiratory effort would likely generate inhalations with different peak inspiratory flowrates through each device (26). Traditionally the examination of DPIs with cascade impactors use methods similar to those described in the United States Pharmacopeia (28), wherein the peak inhalation flowrate of a step-inhalation is chosen to generate a 4 kPa pressure drop across the inhaler. In the present work we instead use semi-realistic inhalation profiles whose magnitudes and durations are chosen to reflect the unique airflow resistance of each DPI.

Specifically, we used the relations of Delvadia et al (26) that model the inhalation flowrate as a sinusoidal function of time (Equations 7 and 8 in (26)), and selected the profiles representative of

the 50th percentile achieved by healthy adults trained on the proper use of DPIs by health care professionals. The time to peak flowrate was taken as the median value reported in (26), 0.49 seconds (which was observed to be independent of device resistance). The duration of inhalation was calculated with Equation 10 in (26) for an inhaled volume of 2.7 l, the median value reported across genders. The peak flowrate was calculated based on the device resistance as per Equation 5 in (26). Table 1 summarizes the peak inhalation flowrate and duration of inhalation for each DPI calculated using the device resistances reported by Delvadia et al (26); additional detail can be found in Ruzycki et al (14). These parameters defining the inhalation patterns correspond to the volumetric flowrate exiting the mouthpiece of each DPI.

DPI performance was characterized using the setup detailed in Figure 1, in which deposition of budesonide from each inhaler was measured in an Alberta Idealized Throat and Next Generation Impactor with pre-separator. A Mixing Inlet (MSP Corporation, Shoreview, MN, USA) was incorporated to allow for the use of time-varying inhalations through DPIs while maintaining a constant inhalation flowrate across the cascade impactor. Airflow through the NGI was set to provide 100 l/min (volumetric) at the inlet of the first stage, and was generated using a vacuum pump (Model 2567-V1; Gast Mfg. Corp., Benton Harbor, MI). This steady flowrate was balanced with a line connected to building supply air such that zero flow developed across the DPI when the breathing machine was not in use. Upon actuation of the breathing machine, airflow from the supply line is reduced in a time-varying manner over the course of an inhalation. As airflow through the NGI is maintained at a constant rate of 100 l/min by the vacuum pump, air is drawn through the DPI to balance the flowrates entering and exiting the mixing inlet, according to conservation of mass.

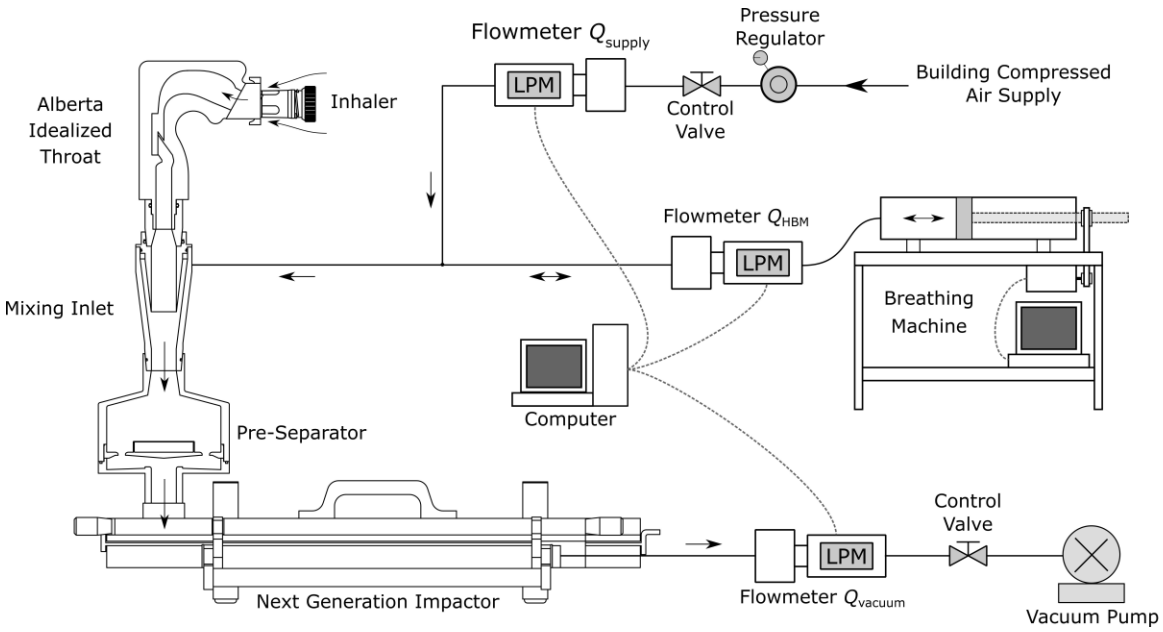

Figure 1: Experimental setup used to quantify deposition from dry powder inhalers. A mixing inlet downstream of the Alberta Idealized Throat allowed for experiments to be conducted with time-varying inhalation profiles while maintaining a constant flowrate through the Next Generation Impactor.

Flowrates (in standard l/min) in the supply, breathing machine, and vacuum lines were measured in 50 msec intervals using thermal mass flowmeters (Model 4043 in the supply and breathing machine lines, Model 4040 in the vacuum line; TSI Inc., Shoreview, MN, USA). The standard flowrate developed across the DPI during an inhalation, $Q_{\mathrm{std,DPI}}(t)$, was calculated from these measurements following the conservation of mass, as shown in Equation 1. Here the subscript std denotes that flowrates are reported in standard l/min, while HBM, vacuum, and supply refer to the breathing machine, vacuum, and supply lines in Figure 1, respectively.

$$Q_{\mathrm{std,DPI}}(t) = Q_{\mathrm{std,HBM}}(t) + Q_{\mathrm{std,vacuum}}(t) - Q_{\mathrm{std,supply}}(t) \quad (1)$$

The volumetric flowrate developed at the exit of the DPI mouthpiece, $Q_{\mathrm{vol,DPI\,exit}}(t)$, was then calculated using Equation 2, which assumes that the relation between the pressure drop and flowrate is quasi-steady and that effects of ambient pressure on inhaler resistance are negligible.

$$Q_{\mathrm{vol,DPI\,exit}}(t) = Q_{\mathrm{std,DPI}}(t)\frac{T_{\mathrm{m}}}{T_{\mathrm{ref}}}\frac{P_{\mathrm{ref}}}{\left(P_{\mathrm{m}} - \left[RQ_{\mathrm{std,DPI}}(t)\frac{T_{\mathrm{m}}}{T_{\mathrm{ref}}}\frac{P_{\mathrm{ref}}}{P_{\mathrm{m}}}\right]^2\right)} \qquad 2$$

T_{m} and T_{ref} denote the measured and reference temperatures (in K), while P_{m} and P_{ref} the ambient and reference pressures (in kPa). Full details regarding the derivations of Equations 1 and 2 are presented in Appendix A.

Calculations were performed in real time using a custom LabVIEW program (LabVIEW Professional Development System 2017; National Instruments, Austin, TX, USA), coded to display the actual inhalation profile generated across the DPI during testing. It is important to note that the inhalation profiles programmed into the breathing machine were similar, but not identical, to those described by Equations 7 and 8 in (26); as noted earlier, Equations 7 and 8 in (26) describe the volumetric flowrate *exiting the mouthpiece* of the DPI. Inhalation profiles input into the breathing machine were calibrated iteratively over the course of several test inhalations to accurately reproduce the unique profiles described by these equations for each DPI. These calibrations were performed with DPIs fixed to the Alberta Idealized Throat to account for potential damping effects of increased airflow resistance on the development of transient inhalation profiles (14).

Prior to each experiment, both halves of the Alberta Idealized Throat, collection surfaces of the pre-separator, and each plate of the NGI were coated with a silicone release spray (Molycote 316; Dow Corning, Midland, MI, USA). Following solvent evaporation (~15 min), these components,

together with the Mixing Inlet, were assembled as shown in Figure 1. Inhaler-specific adapters were fixed to the entrance of the Alberta Idealized Throat to provide airtight seals with each DPI during testing. Adapters were designed such that each DPI was aligned perpendicularly to the plane defining the entrance of the Alberta Idealized Throat, i.e. at an angle of 29° to the transverse plane. With these components in place, the vacuum pump downstream of the NGI was turned on, and the vacuum line flowrate was adjusted to provide a 100 l/min volumetric flowrate at the NGI inlet. Airflow from the supply line was then adjusted to ensure zero airflow developed across the DPI when the breathing machine was not in use.

Five actuations were used for a given inhaler during each experimental run. Prior to each actuation, the inhaler was primed following patient instruction leaflets; Pulmicort Turbuhaler was oriented vertically during priming, Budesonide Easyhaler was shaken up and down repeatedly for 3 to 5 seconds then oriented horizontally prior to priming, and Budelin Novolizer was oriented horizontally as it was primed. The inhaler was then attached to the Alberta Idealized Throat, and the breathing machine was actuated to deliver a single breath through the DPI. The inhaler was removed from the adapter, re-primed, re-attached to the adapter, and re-fired, until five total actuations had been delivered into the setup. As each DPI has a label claim of 200 µg budesonide (see Table 1), the total label claim for each experimental run regardless of inhaler was 1000 µg budesonide.

Components were then disassembled and washed with HPLC grade methanol to provide samples for UV spectroscopy: the Alberta Idealized Throat was washed twice with 10 ml of methanol, the pre-separator was washed three times with 10 ml of methanol, and each plate of the NGI was washed once with 5 ml of methanol. The mass of budesonide in each sample was quantified via UV absorbance relative to standards at 243 nm using a diode array UV-vis spectrophotometer

(Cary 8454; Agilent, Santa Clara, CA, USA). Mass remaining within the DPI following each actuation was not assayed. The above procedure, corresponding to one experimental run, was performed five times with each DPI to allow for statistical comparisons.

Environmental conditions in the laboratory were monitored with a digital hygrometer/thermometer (MI70 Measurement Indicator with HMP75B Humidity and Temperature Probe; Vaisala, Vantaa, Finland). Ambient conditions during testing were as follows: temperature ranged from 22°C to 24°C, relative humidity ranged from 15% to 25%, and absolute pressure ranged from 91 kPa to 94 kPa.

In Vitro Data Analysis

Deposition of budesonide from each DPI (as raw mass, with a total label claim of 1000 µg, equal to 5 actuations from each 200 µg/dose DPI), was summarized using a number of common *in vitro* performance metrics (28–30). Deposition in the Alberta Idealized Throat was considered analogous to extrathoracic deposition *in vivo*. The sum of deposition on the pre-separator and each stage of the NGI was considered analogous to the total dose delivered to the lungs *in vivo* (including any exhaled fraction). Stage cutoff diameters were defined for 100 l/min using manufacturer's correlations. For simplicity, the sum of deposition in the pre-separator and NGI is referred to as the *in vitro* lung dose. Fine particle doses were defined for particles with aerodynamic diameters less than 5 µm. Extra-fine particle doses were defined for particles with aerodynamic diameters less than 2 µm. Mass median aerodynamic diameters and geometric standard deviations, along with fine-particle doses and extra-fine particle doses, were calculated via linear interpolation on particle size distributions (30).

Statistical comparisons of these *in vitro* performance metrics were performed using ANOVA, with post-hoc tests following Tukey's HSD criterion, at a significance level of 0.05. Comparisons were performed in MATLAB (R2018a; The MathWorks Inc, Natick, MA, USA) via the *anova1* and *multcompare* functions.

Lung Deposition

Assuming that the Alberta Idealized Throat approximates the extrathoracic region, the dose exiting the distal end of the Alberta Idealized Throat (i.e. the dose measured in the pre-separator and NGI) represents the *in vivo* total lung dose, while the particle size distribution measured in the pre-separator and NGI represent the initial particle size distribution of aerosol entering the thoracic airways. Here, this *in vitro* data was used as input to a well-established Lagrangian lung deposition model (31,32) to predict respiratory tract deposition from each DPI. Briefly, the model calculates particle deposition on a generational basis in an adult lung geometry consisting of 23 generations (32), with the trachea defined as generation 0, the tracheobronchial tree consisting of generations 0 to 14, and the alveolar region consisting of generations 15 to 23. Deposition mechanisms include inertial impaction, sedimentation, and diffusion during three phases of a breath including inhalation, breath hold, and exhalation. Inhalation parameters were set to equal those used during *in vitro* testing, i.e. an inhaled volume of 2.7 l over a time equal to those noted in Table 1. A breath hold of 10 sec and an exhalation time of 5.4 sec were assumed for each inhaler. In the present study, hygroscopic effects were neglected through the assumption of stable particles.

Particle sizes used in the above correlations were taken as the geometric means of the bracketing cutoff diameters for the *in vitro* masses recovered from the stages of the NGI. The *in vitro* dose depositing in the pre-separator, for which there is no upper size limit, was distributed evenly among the bronchial airways (generations 0 to 8 (33)), given the low likelihood of particles greater than

10.0 μm diameter (the cutoff of the pre-separator at 100 L/min) escaping deposition in these airways for flowrates of interest (34). We weigh the validity of this treatment in the discussion.

Modeling results were considered in terms of regional deposition in the bronchial (generations 0 to 8), bronchiolar (generations 9 to 14), and alveolar (generations 15 to 23) regions, in line with the lung morphology described by the International Commission on Radiological Protection (33). Lung deposition modeling was performed only with the average measurements obtained *in vitro*, and no consideration was given to variations in lung geometry, inhalation patterns, etc. Results should therefore be considered as representative of trends expected to occur in an average adult population, rather than specific to a particular individual.

Airway Surface Liquid Modeling

Material depositing in the tracheobronchial airways is subject to mucociliary clearance. To capture such effects, an airway surface liquid model described in detail elsewhere (19,32,35) was used to predict properties of the airway surface liquid in each generation. Briefly, this model estimates the thickness of the periciliary sol and the mucous layer in each tracheobronchial airway generation for specified values of daily mucous production and tracheal clearance velocity. The periciliary sol and mucous layer are modeled as concentric annular layers. The thickness of the periciliary sol is approximated by the estimated lengths of the cilia lining the airways (35). The mucous layer thickness is estimated via mass conservation and a model of generational mucous clearance velocities based on the specified values of daily mucous production and tracheal clearance velocities (32).

The model predicts, for each tracheobronchial airway generation, the volume of airway surface liquid and the rate of clearance due to mucociliary action (quantified with the first order rate constant $k_{\mathrm{muc,i}}$). Here, the tracheal clearance velocity and daily mucus production were set to 10

mm/min and 10 ml/day, respectively, representative of typical values in healthy adults. For these values, airway surface liquid volumes in the various generations of the tracheobronchial airways fall between 0.11 and 0.36 ml. Airway surface liquid volumes were also considered independent of the amount of dissolved drug, a reasonable assumption for budesonide (having only moderate solubility). First order rate constants describing mucociliary clearance were defined for each generation based on the ratio between the airway surface liquid volumetric flowrate at the trachea and the generational airway surface liquid volume output computed by the airway surface liquid model.

Pharmacokinetic Modeling of Systemic Doses

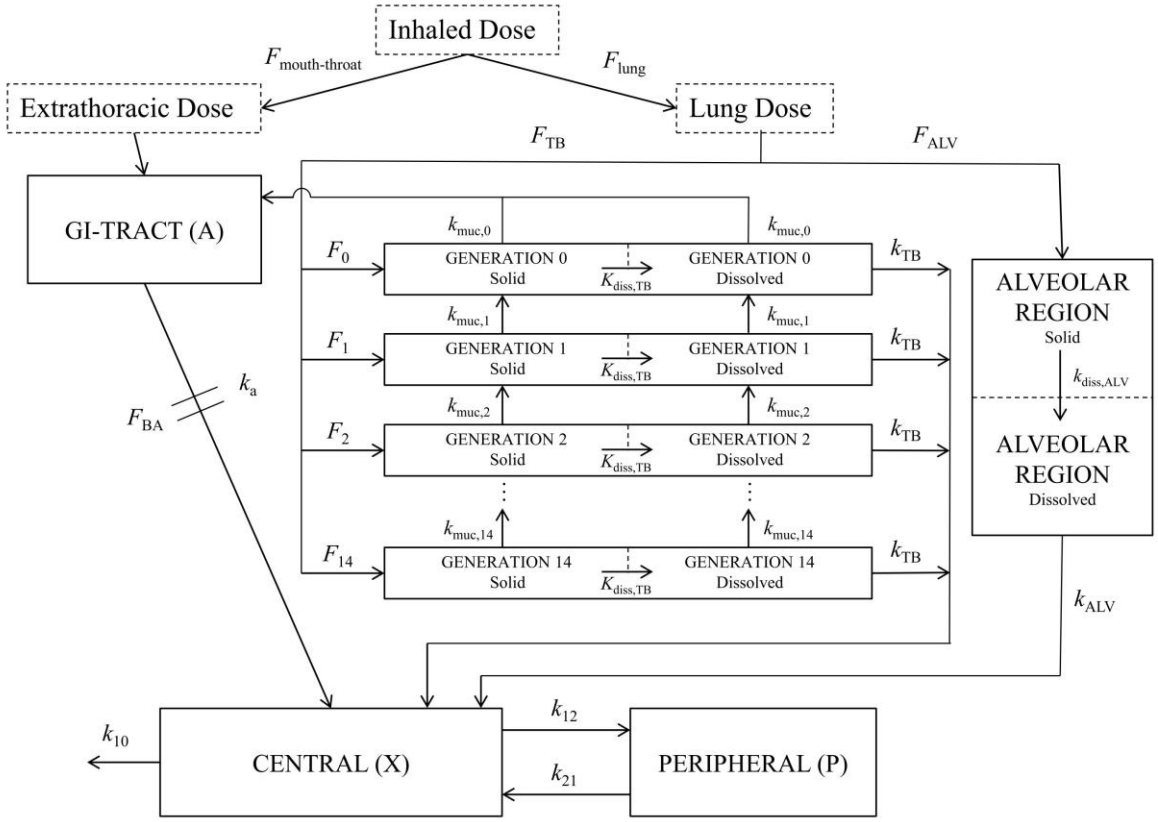

Figure 2: Schematic of the pharmacokinetic model used to predict systemic doses of budesonide from each DPI. First order rate constants k describe the trasition of drug among various compartments. The fraction (F) of the lung dose depositing in each generation of the trachebronchial airways and in the alveolar region is calculated via the lung deposition model. An effective rate constant $K_{\mathrm{diss,TB}}$ is used to model dissolution in the tracheobronchial airways.

A recently developed compartmental disposition model (19) was used to translate predictions of lung deposition into a more traditional measure of drug exposure, i.e. the systemic dose of drug and its evolution over time. This pharmacokinetic model is shown schematically in Figure 2. The lung is comprised of one compartment representing the alveolar region and 15 compartments

representing the tracheobronchial airways. The fraction of the dose of budesonide depositing in each compartment (F) is obtained from the lung deposition model described previously. In each lung compartment, the solid and dissolved portions of drug are considered separately. Solid drug is subject to dissolution in airway surface liquid or alveolar lining fluid. In the alveolar region, this process is described using a first order rate constant $k_{\mathrm{diss,ALV}}$, equal to 17.8 hr^{-1} for budesonide (20), following the study of Weber and Hochhaus (20). In the tracheobronchial airways, particle dissolution is instead modeled as a Nernst-Brunner type diffusion process (36), allowing for the incorporation of effects relating to particle size and drug solubility (see the subsection titled *Dissolution Model in the Tracheobronchial Airways*). Mucociliary clearance, which acts to shuttle both dissolved and solid budesonide from deeper generations of the tracheobronchial airways towards the trachea, is characterized by first order rate constants, $k_{\mathrm{muc,i}}$ (ranging from 1.8 to 5.4 hr^{-1}, as derived from the airway surface model discussed above), estimated from the airway surface liquid model. Dissolved budesonide is subject to absorption from the alveolar region according to the rate constant k_{ALV}, estimated as 20 hr^{-1} (20), and from each generation of the tracheobronchial airways according to the rate constant k_{TB}, estimated as 10 hr^{-1} (20). As discussed by Weber and Hochhaus (20), these rate constants are arbitrarily chosen to represent fast absorption of a lipophilic substance from the alveolar region, and slightly slower absorption from the tracheobronchial airways.

A separate compartment representing the gastrointestinal tract accounts for the dose depositing in the extrathoracic region (here measured *in vitro* with the Alberta Idealized Throat) and drug removed from the lungs via mucociliary clearance. Absorption of budesonide from the gastrointestinal compartment is governed by the oral bioavailability F_{BA}, 0.107 (37), and the rate constant k_{a}, 0.45 hr^{-1} (20). Two cases were considered for each DPI, the first using the oral

bioavailability for budesonide from the literature (as above), and the second with the oral bioavailability set to zero to simulate the effects of a continual charcoal block, given the use of this technique in some pharmacokinetic studies *in vivo*.

The body itself is represented with a standard two compartment central-peripheral model, with the central compartment consisting of blood and well-perfused organs, and the peripheral compartment consisting of poorly perfused tissues. Drug transfer between these compartments is governed by rate constants k_{12} and k_{21}, equal to 20.01 hr^{-1} and 11.06 hr^{-1} for budesonide, respectively (20). Other general pharmacokinetic parameters are as follows. The volume of distribution at steady state, $V_{\mathrm{d,SS}}$, was set as 183 l (38,39). Clearance, CL, was taken as 83.7 l/h (37). The volume of the central compartment, V_{C}, was calculated to be 65.1 l from Equation 3, adapted from Yates and Arundel (40). Finally, the elimination rate constant k_{10}, 1.29 hr^{-1}, was calculated by dividing the clearance by the volume of the central compartment, i.e. $k_{10} = CL/V_{\mathrm{C}}$ (40), under the assumption that elimination occurs entirely from the central compartment.

$$V_{\mathrm{C}} = \frac{V_{\mathrm{d,SS}}}{1 + \frac{k_{12}}{k_{21}}} \qquad 3$$

Dissolution Model in the Tracheobronchial Airways

Drug dissolution is commonly modelled as a Nernst-Brunner process (41), which combines the diffusion layer concept with Fick's second law of diffusion. For Nernst-Brunner dissolution, the limiting step that governs how dissolution proceeds is the diffusion of molecules across a stagnant film of liquid (the diffusion layer) surrounding submerged solids. The general equation describing this process, when written in terms of the mass of solid material m at time t, is shown in Equation 4.

$$\frac{dm}{dt} = -\frac{DS}{h}(c_s - c(t)) \quad (4)$$

D is the diffusion coefficient of the substance in the solvent, S is the surface area of submerged solids, h is the diffusion layer thickness, c_s is the solubility of the substance in the solvent, and $c(t)$ is the concentration of the substance in the solvent outside of the diffusion layer at a particular time.

In the present work, we assumed that particles depositing in the tracheobronchial airways are quickly drawn into the airway surface liquid and are submerged fully (42), and that the subsequent dissolution of said particles is governed by a Nernst-Brunner process. Equation 4 was recast in terms of an effective rate constant $K_{diss,TB}$, and was applied to the mass of solid (undissolved) drug in each specific generation (m_i, itself varying with time), as per Equation 5.

$$\frac{dm_i}{dt} = -K_{diss,TB} m_i(t)(c_s - c(t)) \quad (5)$$

The effective rate constant $K_{diss,TB}$ was expressed in terms of the particle geometric median diameter $d_{g,50}$ (calculated from *in vitro* measurements of MMADs, assuming spherical particles), particle density ρ_P (1270 kg/m^3 for budesonide), solubility of micronized budesonide in the airway surface liquid (16 µg/mL (43)), and the diffusion coefficient D (6.19×10^{-6} cm^2/min for budesonide in water at 37 °C (36)) as per Equation 6.

$$K_{diss,TB} = \frac{12D}{\rho_P d_{g,50}^2} \quad (6)$$

This expression for $K_{diss,TB}$ assumes that the diffusion layer thickness h was equal to the particle radius (valid for particle radii smaller than 30 µm (36,44)) and that the total surface area and the mass of particles are well-approximated by particles with the geometric median diameter. As a

further simplification, $K_{diss,TB}$ was assumed to be constant with time. These assumptions, and their influence on the systemic dose, are considered in the discussion. The effective rate constant was calculated individually for each DPI based on our *in vitro* measurements.

The pharmacokinetic model described above yielded a system of ordinary differential equations describing the mass of drug in each compartment over time. Full details regarding these equations are provided in Appendix B. This system was solved in spreadsheet format in Microsoft Excel using explicit Euler time advancement over a 24-hour period, with uniform timesteps of 0.01 hr to achieve timestep-independent results (19). Standard pharmacokinetic parameters including the area under the curve in 24 hours (AUC_{24}), the maximum concentration ($c_{\max}$), and the time to maximum concentration ($t_{\max}$) were determined from the calculated distributions. The present model did not consider variations in parameters (like the volume of distribution, absorption rates, clearance, etc.) as would occur in a population. Like the lung deposition model, results should be considered representative of trends occurring in an average adult population, rather than being specific to a particular individual. We consider the feasibility of incorporating variability in the above models in the discussion.

The *in vivo* pharmacokinetics of inhaled budesonide have been well-studied in the literature, particularly with Pulmicort Turbuhaler. Systemic concentrations as estimated in the present work were compared to a number of *in vivo* pharmacokinetic studies of inhaled budesonide in healthy or mildly asthmatic adults, including those by Thorsson, Edsbäcker, and Conradson (38) (1000 µg via Turbuhaler, with and without charcoal block), Argenti, Shah, and Heald (45) (600 µg via Turbuhaler), Duddu et al (46) (800 µg via Turbuhaler, with charcoal block), Harrison and Tattersfield (47) (1200 µg via Turbuhaler), Lähelmä et al (48) (1000 µg via Turbuhaler and Easyhaler, with charcoal block), Möllmann et al (49) (1000 µg via Turbuhaler), Thorsson et al

(50) (1000 µg via Turbuhaler), Mortimer et al (51) (800 µg via Turbuhaler), and Hämäläinen et al (52) (800 µg via Turbuhaler and Easyhaler) to validate model estimates of the systemic dose. For Budelin Novolizer, no pharmacokinetic data was found in the literature aside from single data points in two summary of product characteristics (SmPCs), one from the UK (53) and one from Slovenia (54), which are included for completeness. *In vivo* pharmacokinetic profiles were scaled, where necessary, to a dose of 1000 µg under the assumption of dose linearity for inhaled budesonide (55). *In vivo* data reported in molar units was transformed to a gram-basis using the molecular weight of budesonide, 430.534 g/mol.

Results

Particle size distributions of budesonide measured *in vitro* are shown in Figure 3. A summary of relevant *in vitro* parameters, including the doses of budesonide measured in the Alberta Idealized Throat and in the NGI and pre-separator, is provided in

Table 2. Significant differences, denoted by dashed bars in

Table 2, are evident. Deposition in the Alberta Idealized Throat was significantly different for all DPIs (ANOVA; $p < 0.0001$), ranging from 398.0 µg with Turbuhaler to 1041.0 µg with Easyhaler. The *in vitro* lung dose was greatest with Turbuhaler (at 439.8 µg), almost twice the amount measured with Easyhaler (228.2 µg, $p < 0.0001$) or Novolizer (261.3 µg, $p < 0.0001$). The comparison of *in vitro* lung dose between Easyhaler and Novolizer was the only comparison here that failed to reach statistical significance ($p = 0.2816$). For mass median aerodynamic diameter, Easyhaler (3.62 µm) yielded larger particles than Turbuhaler (2.18 µm, $p < 0.0001$), which in turn yielded slightly larger particles than Novolizer (1.94 µm, $p = 0.0069$). The fine particle and extra fine particle doses were considerably smaller for Easyhaler (169.1 µg and 79.6 µg, respectively)

than observed with the other inhalers. For Novolizer, most of the *in vitro* lung dose was contained in extra-fine particles, with an extra-fine particle dose of 210.1 µg.

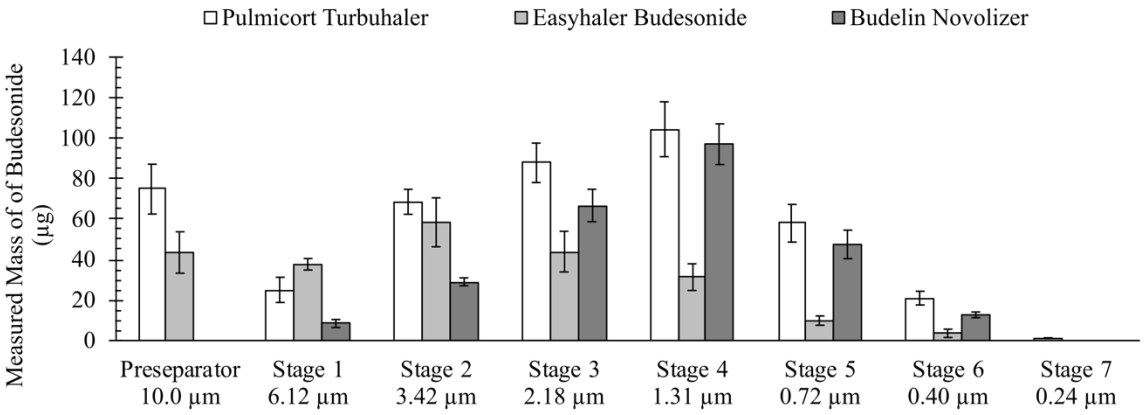

Figure 3: Particle size distributions measured downstream of the Alberta Idealized Throat with each DPI, expressed as the average mass of budesonide measured on the pre-separator and each stage of the Next Generation Impactor. Cutoff diameters correspond to operation of the NGI at 100 l/min. Error bars denote standard deviation.

Table 2: Summary of *in vitro* measurements and performance metrics, expressed as average ± standard deviation (n = 5). Significant differences are represented by dashed bars.

Parameter	Pulmicort Turbuhaler	Easyhaler Budesonide	Budelin Novolizer
Delivered Dose (µg)	837.8 ± 57.0	1269.3 ± 92.1	988.7 ± 34.7
Alberta Idealized Throat Deposition (µg)	398.0 ± 24.4	1041.0 ± 119.2	727.4 ± 44.5

Next Generation Impactor + pre-separator Deposition (µg)	439.8 ± 36.8	228.2 ± 32.6	261.3 ± 27.7
Fine Particle Dose, < 5 µm (µg)	354.6 ± 40.1	169.1 ± 34.1	257.8 ± 27.7
Extra-fine Particle Dose, < 2 µm (µg)	253.3 ± 30.8	79.6 ± 18.7	210.1 ± 24.2
Mass Median Aerodynamic Diameter (µm)	2.18 ± 0.08	3.62 ± 0.15	1.94 ± 0.02
Geometric Standard Deviation (-)	2.09 ± 0.03	1.99 ± 0.04	1.76 ± 0.01

The *in vitro* differences summarized in

Table 2 manifested in differences in calculated regional lung deposition, as shown in Figure 4. Calculated bronchial deposition (generations 0 to 8) ranged from 117 µg with Turbuhaler to 27 µg with Novolizer. Calculated alveolar deposition also ranged considerably, from 263 µg with Turbuhaler to 116 µg with Easyhaler. In contrast, calculated deposition in the bronchiolar region (generations 9 to 14) was more comparable between inhalers, ranging from 37 µg with Turbuhaler to 24 µg with Novolizer.

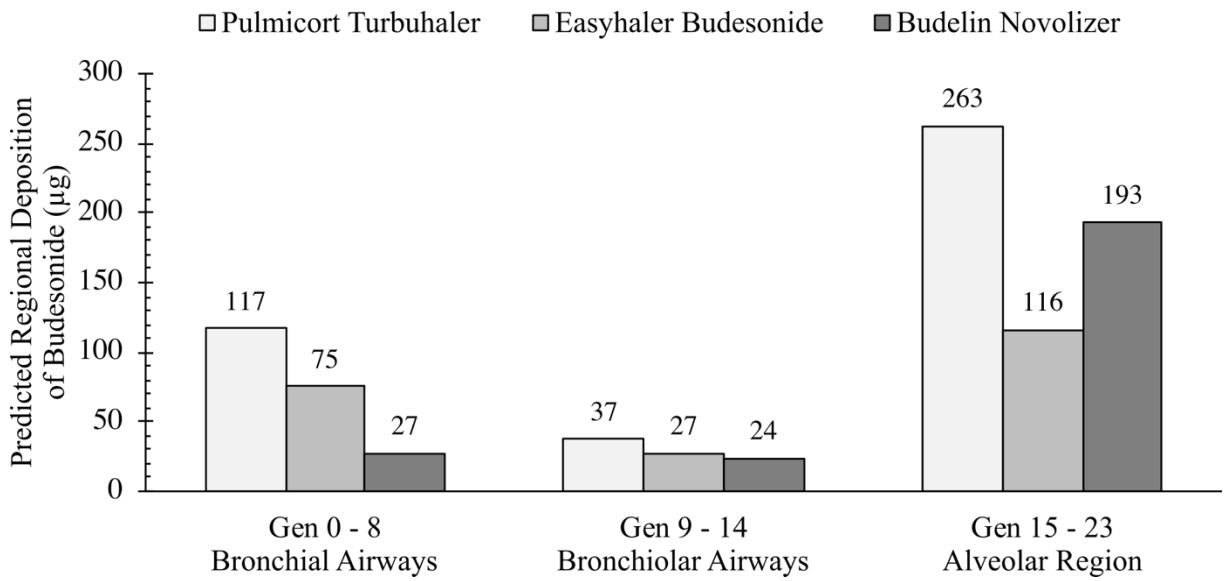

Figure 4: Calculated regional lung deposition of budesonide based on the particle size distributions measured *in vitro* (Figure 3) and the inhalations defined in Table 1 for the adult lung geometry of Finlay et al (32).

For the prediction of systemic dose, the effective rate constant $K_{\mathrm{diss,TB}}$ was first calculated for each DPI based on the *in vitro* data using Equation 6, yielding 93.4, 34.0, and 118.0 m^3/kg·hr for Turbuhaler, Easyhaler, and Novolizer respectively. The system of equations comprising the model was then solved numerically. The resulting systemic profiles are shown in Figure 6, together with *in vivo* data from the literature for Turbuhaler (38,47–49), Easyhaler , and Novolizer. As noted in the methods, data was scaled to an effective dose of 1000 µg when necessary under the assumption of dose linearity for inhaled budesonide (55).

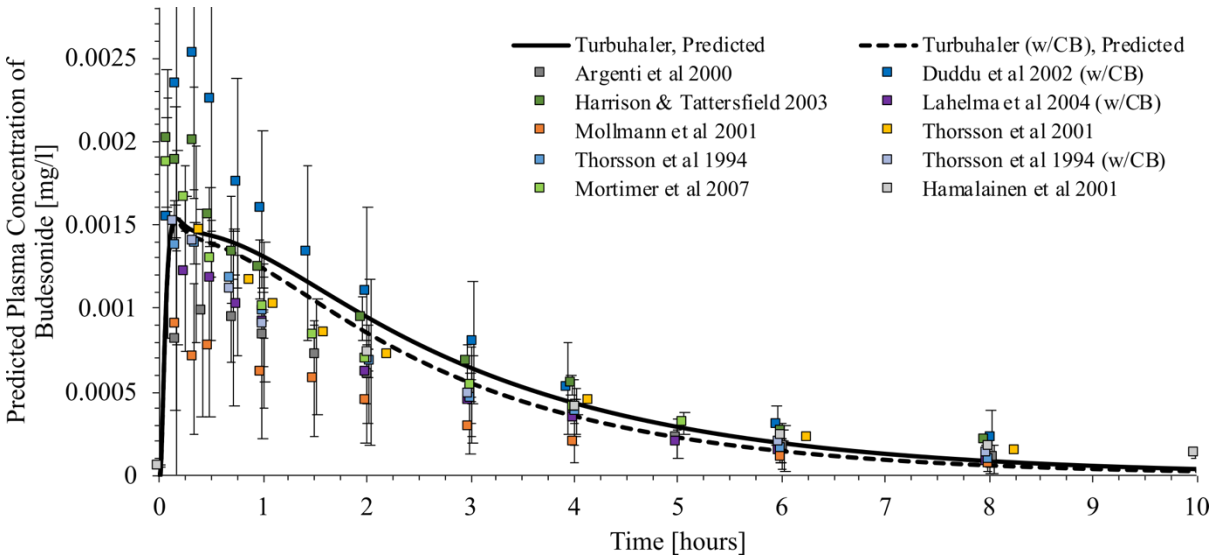
Turbuhaler, Predicted
Turbuhaler (w/CB), Predicted
Argenti et al 2000
Duddu et al 2002 (w/CB)
Harrison & Tattersfield 2003
Lahelma et al 2004 (w/CB)
Mollmann et al 2001
Thorsson et al 2001
Thorsson et al 1994
Thorsson et al 1994 (w/CB)
Mortimer et al 2007
Hamalainen et al 2001
Predicted Plasma Concentration of Budesonide [mg/l]
0.0025
0.002
0.0015
0.001
0.0005
0
0 1 2 3 4 5 6 7 8 9 10
Time [hours]

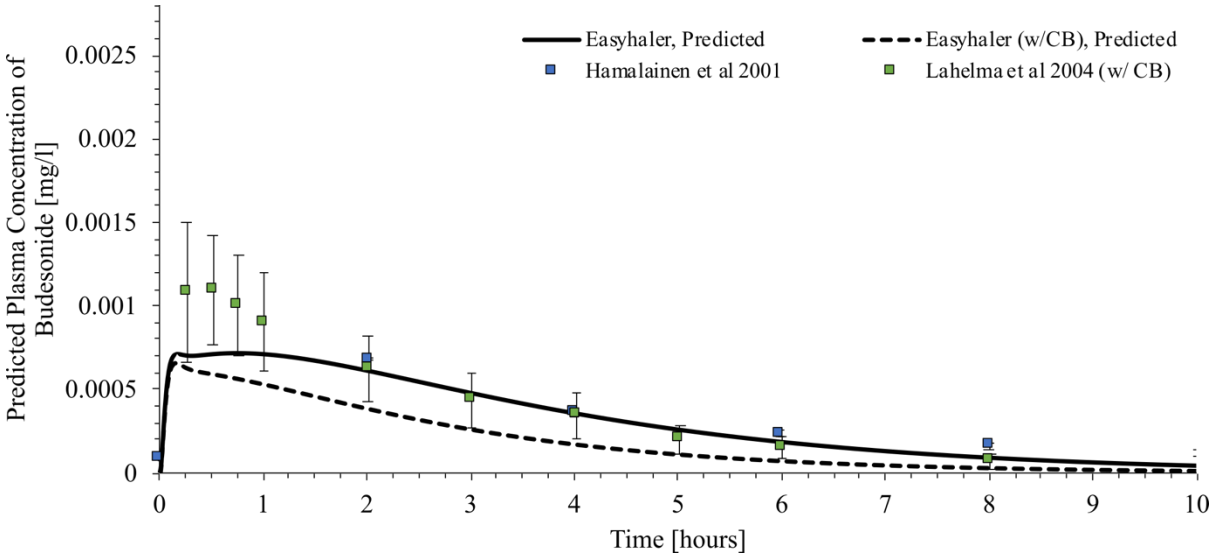
Easyhaler, Predicted
Easyhaler (w/CB), Predicted
Hamalainen et al 2001
Lahelma et al 2004 (w/ CB)
Predicted Plasma Concentration of Budesonide [mg/l]
0.0025
0.002
0.0015
0.001
0.0005
0
0 1 2 3 4 5 6 7 8 9 10
Time [hours]

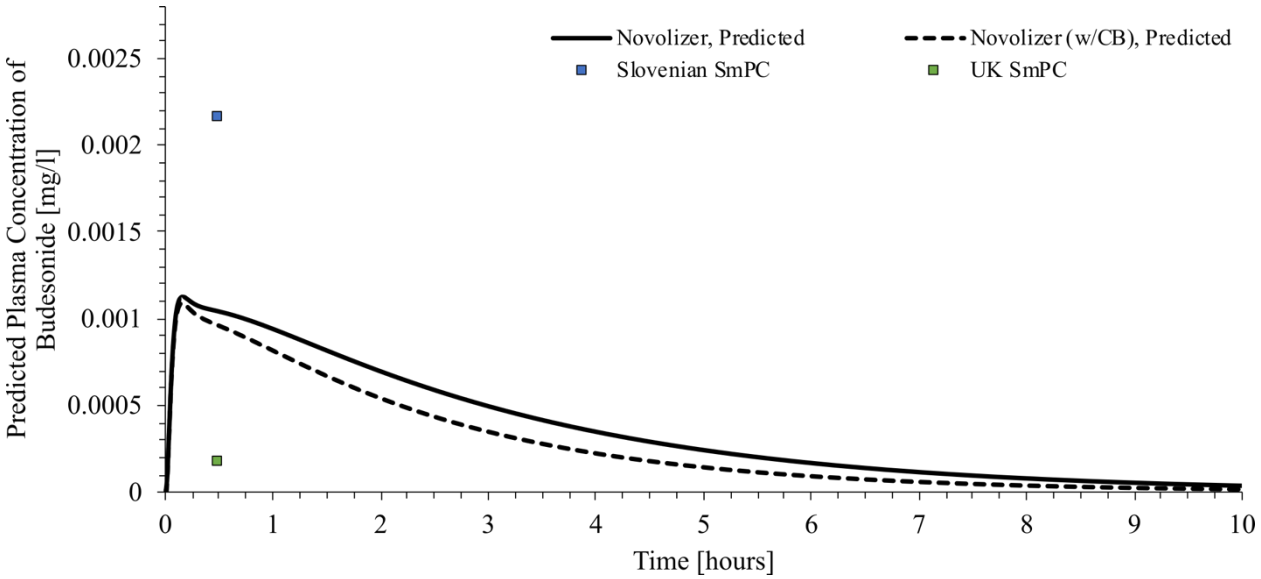

Figure 5: Calculated plasma concentrations with and without oral absorption for (top) Pulmicort Turbuhaler (middle) Easyhaler Budesonide and (bottom) Budelin Novolizer. *In vivo* data from the literature scaled, when necessary, to a dose of 1000 µg budesonide (w/CB = with charcoal block).

Standard pharmacokinetic parameters are presented in Table 3. For the case where no charcoal block was simulated, Turbuhaler was estimated to yield the largest area under the curve in 24 hours, at 4.87 µg·hr/l, with Easyhaler and Novolizer yielding smaller values of 3.34 and 3.73 µg·hr/l, respectively. In terms of systemic concentration, Easyhaler Budesonide demonstrated two peaks of similar values, 0.71 µg/l at 0.17 hr and 0.72 µg/l at 0.75 hr. Turbuhaler yielded the highest estimated peak concentration, at 1.54 µg/l, while Novolizer fell in the middle, at 1.13 µg/l. Time to peak concentration was the same for each DPI (0.16 to 0.17 hr). For predictions with charcoal block, the AUC decreased considerably with each inhaler, while the peak systemic concentration remained similar. The double peak occurring with Easyhaler Budesonide disappeared in the simulation with charcoal block.

Table 3: Summary of calculated pharmacokinetic parameters for each DPI. w/o CB = without charcoal block, w/ CB = with charcoal block.

DPI	Area Under the Curve, 24 hours AUC_{24} (µg·hr/l)		Peak Systemic Concentration c_{max} (µg/l)		Time to Peak Concentration t_{max} (hr)	
	w/o CB	w/ CB	w/o CB	w/ CB	w/o CB	w/ CB
Pulmicort Turbuhaler	4.87	4.29	1.54	1.52	0.16	0.16
Easyhaler Budesonide	3.34	1.94	0.71 / 0.72*	0.66	0.17 / 0.75*	0.16
Budelin Novolizer	3.74	2.79	1.13	1.09	0.16	0.16

* Easyhaler Budesonide demonstrated two peaks in the simulation without charcoal block, the second peak being denoted by asterisk.

Discussion

In the present study, we use *in silico modeling to* extend *in vitro* measurements of DPIs to predict regional lung deposition and systemic exposure. To illustrate the method, three marketed budesonide DPIs spanning a range of device characteristics were selected for testing. The *in vitro* results presented herein demonstrate considerable *in vitro* differences in performance between these DPIs (see

Table 2); however *in silico* modeling permitted estimation of how these differences may or may not result in differences in regional deposition or in pharmacokinetic parameters, such as systemic dose and peak concentration. Several interesting observations arising through these combined *in vitro – in silico* methods are discussed below.

The *in vitro* measurements indicate that despite having the same label claim of 200 µg budesonide, there is variation in the amount of drug leaving the mouthpiece between the DPIs when tested with semi-realistic inhalation profiles. Delivered doses ranged from 837.8 µg with Turbuhaler (167.6 µg per actuation) to 1269.3 µg with Easyhaler (253.9 µg per actuation), and are in excellent agreement with a recent paper by our group using the same inhalers in a different experiment (14). Such differences in DPI output compared to the label claim are well documented in the literature (27), and may be partly explained by batch-to-batch variation. Of note is the agreement of our measured MMADs with values in the literature for each DPI (56–58). Parisini et al measured an MMAD for Easyhaler Budesonide of 3.92 ± 0.24 µm (average ± standard deviation) with the NGI plus pre-separator following compendial methods, versus 3.62 ± 0.15 µm measured here (56). Yoshida et al measured an MMAD for Pulmicort Turbuhaler of 2.20 ± 0.06 µm with the NGI plus pre-separator at a flowrate of 75 L/min, versus 2.18 ± 0.08 µm measured here (57). Wei et al measured an MMAD for Budelin Novolizer of 1.86 ± 0.06 µm with the NGI (without pre-separator) downstream of their anatomical VCU medium mouth-throat model with a realistic inhalation similar to that used in the present work, versus 1.94 ± 0.02 µm measured here (58). Our match to the data of Parisini et al (56) with Easyhaler Budesonide and Yoshida et al (57) for Pulmicort Turbuhaler despite our use of the Alberta Idealized Throat and their use of the United States Pharmacopeia Induction Port (USP-IP) can be explained through the action of the pre-separator. The USP-IP is known to significantly underestimate mouth-throat deposition, but the inclusion of the pre-separator means that larger particles that would deposit within the extrathoracic tract *in vivo* are removed by the pre-separator prior to entering the NGI itself. In the present work, the Alberta Idealized Throat acts as an analogue of the extrathoracic region (14), allowing for a deeper interpretation of the dose depositing on the pre-separator. The observation

of a considerable dose on the pre-separator for Pulmicort Turbuhaler and Easyhaler Budesonide implies that a non-negligible dose of large particles penetrates past the extrathoracic region for some DPIs. This does not appear to be the case with Budelin Novolizer; here the dose recovered from the pre-separator with this inhaler was below quantifiable limit while only 8.4 ± 2.0 μg of budesonide were recovered from plate 1. This corroborates well with the measurement of less than 5 μg on the first plate of the NGI (without pre-separator) from Budelin Novolizer by Wei et al (58) downstream of their anatomical throat model. A proper investigation of the penetration of large particles through the Alberta Idealized Throat during a realistic inhalation requires additional experimentation with a measurement technology that can size large particles over a time-varying inhalation, e.g. time-of-flight aerodynamic sizers or laser light scattering systems.

Of more interest to the present discussion is how *in vitro* differences in delivered dose and particle size distributions result in more clinically relevant measures. Predicted lung deposition, shown in Figure 4, lends evidence to the notion that differences in performance *in vitro* can result in large differences in lung deposition. For Turbuhaler, relatively small particles (MMAD of 2.18 ± 0.08 μm) coupled with a large *in vitro* lung dose resulted in a large predicted alveolar dose of 263 μg. For Easyhaler, larger particles (MMAD of 3.62 ± 0.15) coupled with a decreased *in vitro* lung dose resulted in a much smaller predicted alveolar dose of 116 μg. For Novolizer, whose *in vitro* lung dose was not significantly different than Easyhaler (261.3 vs 228.2 μg respectively; $p = 0.2816$), small particle sizes (MMAD of 1.94 ± 0.02 μm) resulted in increased alveolar deposition (at 193 μg). One factor to bear in mind with the above interpretation lies in the treatment of the un-sized portion of the *in vitro* lung dose, i.e. the dose measured in the pre-separator. As noted in the methods, the dose measured on the pre-separator was distributed evenly among the bronchial airways (corresponding to generations 0 to 8 in the present lung model), based on the low

likelihood of particles greater than 10 µm (the cutoff of the pre-separator at 100 l/min) escaping deposition in these airways at flowrates of interest. For example, at a flowrate of 60 L/min (less than the peak value used with each DPI in the present work), more than 60% of particles with an aerodynamic diameter of 10 µm are predicted to deposit in generations 0 to 8 based on the correlation of Chan & Lippmann (34). For 15 µm particles, deposition in these airways increases to more than 90%. This treatment, though rudimentary, allows for the consideration of this dose without assigning an arbitrary upper particle size (note that while deposition in the Alberta Idealized Throat has been well-characterized (59,60), the time varying inhalations developed through the throat in the present setup preclude the definition of a useful "throat cutoff diameter," or upper size limit for the initial thoracic dose, and such a "throat cutoff diameter" would be rather coarse compared to a well-designed impactor plate regardless). It is this un-sized dose that dominates the bronchial deposition of Turbuhaler and Easyhaler in the present model, especially when compared to Novolizer, for which deposition measured in the pre-separator was below quantifiable limit. As noted above, a thorough investigation of this effect requires use of a different measurement technique than cascade impaction. A takeaway is that one should consider both the sized and un-sized portions of the dose measured *in vitro* in predicting lung deposition; the MMAD alone may not be sufficient in describing regional lung deposition from inhalers.

Our predictions of a small deposition fraction in the bronchiolar airways (generations 9 to 14 in the present lung model) are consistent with the known difficulty in targeting deposition to these small conducting airways (61). Some have suggested that inhaled corticosteroids like budesonide may provide increased therapeutic benefit when targeted to the small airways (62–64). Estimated bronchiolar deposition is similar for these DPIs despite their performance spanning a range of *in vitro* characteristics, suggesting that particle size and device design can only go so far in targeting

delivery to certain lung regions. Optimizing delivery beyond the limits of these conventional approaches may require more sophisticated techniques. Two potential approaches include pulsed bolus delivery (65) and enhanced condensational growth (66), though both techniques require technology beyond what is used in typical passive DPIs.

The lung deposition model used herein does not account for bolus effects, and thus some differences in deposition between that calculated here and what occurs *in vivo* may be expected to occur. Bolus emission of aerosols from DPIs has been studied numerically (67), but the distribution of particles within the bolus (in terms of number and size) is not well-characterized, precluding the use of more advanced deposition modeling that incorporate bolus effects. It is also tempting to draw direct comparisons between predictions of deposition in the tracheobronchial airways and alveolar region with central-peripheral deposition measured via scintigraphy *in vivo*, some data of which exists for these inhalers (68–71). However, a direct one-to-one correlation is not possible owing to inherent difficulties in registering radioactivity to specific anatomical areas in the lungs, particularly with 2-dimensional scintigraphy data (72).

Beyond predictions of regional lung deposition, the present methodology further allows for the modeling of systemic dosing based on the location of deposition in the lung. Calculated systemic concentrations of budesonide, shown in Figure 5, and the peak systemic concentrations and area under the curves, shown in Table 3, are in good agreement with data from the literature (38,45–52), suggesting the present methodology provides reasonable estimates of typical *in vivo* measures of inhaler performance. A number of observations can be made on the relationship between calculated regional lung deposition and pharmacokinetic parameters, as shown in Figure 6 (wherein simple linear regression was performed in Excel for the purposes of illustration) for the case where absorption from the gastrointestinal tract was considered. Firstly, peak systemic

concentration correlates extremely strongly with the alveolar dose (R^2 = 0.9994, Figure 6 (a)), while a weaker correlation is obtained between peak systemic concentration and the total lung dose (R^2 = 0.8414, Figure 6 (c)). This is attributable to the rapid uptake of budesonide modeled from the alveolar compartment (k_{ALV} = 20 hr^{-1} (20)) as compared to the tracheobronchial region (k_{TB} = 10 hr^{-1} (20)), but also depends on the rate of dissolution for particles depositing in the alveolar liquid lining fluid versus the airway surface liquid in the tracheobronchial airways. In the present model, dissolution and uptake occurs more rapidly in the alveolar region than in the tracheobronchial region, with the end result being that the peak systemic concentration is dependent primarily on the dose depositing in the alveolar region. In contrast, the area under the curve shows a closer correlation with the total lung dose (R^2 = 0.9821, Figure 6 (d)) than with the alveolar dose (R^2 = 0.9182, Figure 6 (b)). Consideration of only the alveolar dose misses the significant contribution of absorption from the tracheobronchial airways that occurs over longer timespans. Figure 6 (e) and (f) show that neither the peak systemic concentration nor the area under the curve are well-correlated with deposition in the tracheobronchial region (generations 0 to 14). In this region mucociliary clearance shunts a portion of the tracheobronchial dose into the gastrointestinal tract, where the low bioavailability of budesonide limits its contribution to the systemic dose. These standard pharmacokinetic parameters, therefore, do not appear to provide much useful information on the deposition of budesonide specifically in the tracheobronchial airways. Such may be the case with other inhaled therapeutics with limited solubility in airway surface liquid and low oral bioavailability. In the pulmonary biopharmaceutical classification system proposed by Hastedt et al (43), budesonide lies close to the critical band defining a dissolution-limited drug (budesonide itself is not considered dissolution-limited owing to its moderate solubility). We suspect that our finding of limited correlation between tracheobronchial

deposition and pharmacokinetic measures of peak systemic concentration and area under the curve extends to dissolution-limited drugs with low oral bioavailability (e.g. beclomethasone dipropionate, fluticasone propionate, among others (43)), wherein mucociliary clearance removes much of the tracheobronchial dose before dissolution and absorption can occur.

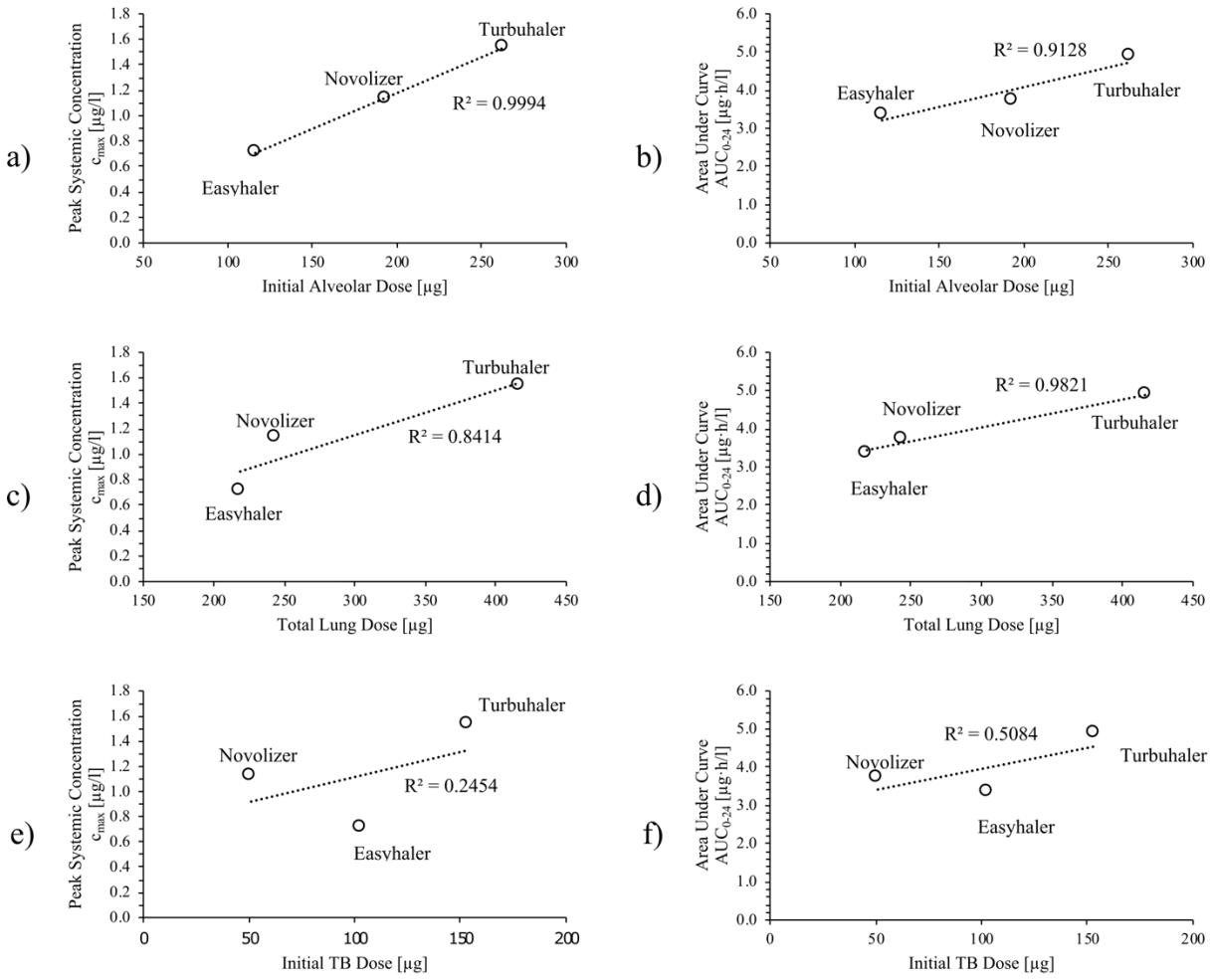

Figure 6: Correlations between calculated regional deposition and predicted pharmacokinetic parameters, including (a) peak systemic concentration versus initial alveolar dose, (b) area under curve versus initial alveolar dose, (c) peak systemic concentration versus total lung dose, (d) area under curve versus total lung dose, (e) peak systemic concentration versus tracheobronchial dose, and (f) area under the curve versus tracheobronchial dose, considering absorption from the gastrointestinal tract.

The present pharmacokinetic model assumes that dissolution in the tracheobronchial airways can be modeled using a Nernst-Brunner diffusion process, but does not extend this assumption to the alveolar region. In a Nernst-Brunner process, particles are assumed to be fully submerged and are surrounded by a stagnant diffusion layer with a thickness comparable to the particle size. The assumption of full submersion may be reasonable in the conducting airways, where the airway surface liquid is sufficiently deep (43), and where surface tension acts to quickly draw deposited particles into the aqueous subphase below the mucous layer (42). Regarding the assumption of stagnant diffusion layers surrounding submerged particles, we suppose that the beating action of cilia, which must induce some motion in the airway surface liquid to facilitate clearance (73), is a complicating factor that may require a deeper analysis. In the much thinner alveolar lining fluid (~ 0.2 μm (43)), the assumptions of full submersion of a particle and the presence of a diffusion layer of comparable thickness are more tenuous, meaning that the kinetics of dissolution in the alveolar region are probably not well-described with a classical Nernst-Brunner process. Others have suggested using modified Nernst-Brunner processes to describe dissolution in the alveolar region (74,75); the most sophisticated of these models necessitates experimental determination of wettability (74). However, an analytical model of dissolution in the extremely thin alveolar fluid has thus far eluded development. As the validity of these approaches remains to be determined, we defer to a simpler model based on *in vivo* data that models alveolar dissolution with a first order rate constant (20). Considering that each DPI used here delivers micronized budesonide, and that particles that deposit in the alveolar region will have similar diameters, we do not expect considerable differences between these DPIs in dissolution behavior, due to e.g. solubility, that are not captured by this treatment. The agreement between our model outputs and the available *in vivo* data suggests this is a reasonable approximation for micronized budesonide. For novel drugs and

formulations, validated models of dissolution in the alveolar region are required before *a priori* prediction of drug disposition can be accurately performed from first principles.

The advantage of modeling dissolution as a Nernst-Brunner process arises from the ability to predict how changes to formulation factors like drug solubility and particle size influence *in vivo* performance. Experimental measurements of dissolution and solubility (36,76) can be incorporated into the present model to inform how changes in formulation affect dissolution rates and absorption in the tracheobronchial airways. Dissolution testing suggest that there is some time-dependence to the thickness of the diffusion layer surrounding particles (36), but the exact form of this time-dependence is unknown. Here we have assumed that the dissolution rate is constant with time, which will underestimate the speed of dissolution in the tracheobronchial region. As our modeling suggests that the alveolar dose is the driver of the peak systemic concentration, such effects are less important in the context of systemic pharmacokinetics than they are in the determination of local drug concentrations in the airway surface liquid, a topic to be explored in future work.

As noted by Weber and Hochhaus (20), the rate constants used to model absorption from the alveolar and tracheobronchial airways were chosen arbitrarily. Physiologically-based pharmacokinetic modeling could be incorporated to inform these rate constants based on experimental measurements of membrane permeabilities and tissue retention, along with estimates of membrane surface areas and blood volumes in relevant regions of the lungs, as has been explored in a number of recent publications (74,75,77). Noting that it remains unclear as to how best to implement the results of various methods for assessing drug permeability with absorption in different regions of the lung (78), and considering the general agreement between the predictions from our model and the *in vivo* data for Turbuhaler, the rate constants of Weber and Hochhaus

(20) appear reasonable in the place of more advanced physiologically-based pharmacodynamic modeling for our purposes, especially as the mathematical relationships between absorption rates and drug masses in these various models are similar. Advanced modeling techniques will certainly be indispensable, however, in extending the utility of the present methodology towards novel drugs and formulations.

A comparison of the estimated systemic concentrations with and without charcoal block, from Figure 5 and Table 3, suggests that despite the low oral bioavailability of budesonide a non-negligible amount of drug enters systemic circulation through the gastrointestinal tract (via either the initial extrathoracic dose or dose removed from the conducting airways through mucociliary clearance). This effect is more important for inhalers that demonstrate higher extrathoracic deposition. For inhaled corticosteroids, wherein systemic pharmacokinetic data is often considered as indicative of the level of adverse side effects, use of a charcoal block during *in vivo* testing to estimate equivalence of the lung dose (79) will mask these effects.

Available clinical evidence suggests that the budesonide DPIs used in the present work are similarly efficacious in the treatment of asthma (80–82). The similarity of the dose delivered to the small conducting airways may play a role here given the hypothesized importance of delivery to this region for efficacious action of inhaled corticosteroids (62–64). Other factors to consider include whether the doses delivered to target tissues from these DPIs lie on the plateau of the dose-response curve, and whether the clinical studies used to evaluate equivalence are sufficiently powered to be able to identify any clinically meaningful difference. It is important to note that the present model does not allow for the prediction of local effects of deposited drug; a deeper interpretation of local therapeutic effects of inhaled corticosteroids requires the implementation of more advanced physiologically-based pharmacokinetic modelling (74,75,77) together with

pharmacodynamics. Budesonide itself poses an interesting problem here, as there is evidence of fatty-acid esterification and subsequent re-release of budesonide from lung tissue (83) that complicates drawing conclusions on local drug action based on free drug concentrations in the airway surface liquid post-dosing. Nevertheless, promising developments in models of drug action have recently been described (see e.g. the receptor occupancy model for inhaled corticosteroids described by Shao et al (84)), and such models could be incorporated to the current methodology to expand its usefulness towards novel formulations.

Another limitation of the present work relates to the absence of estimates of variability in regional deposition or pharmacokinetic profiles. Extension of the present model to incorporate some inherent randomness in parameter values in the form of stochastic lung deposition modeling and population pharmacokinetics remains a topic for future work. In principle, one could couple *in vitro* testing to stochastic models of lung deposition and population pharmacokinetics to ultimately predict clinical metrics in a population. This approach is not trivial, however, as variability in one step should inform variability in subsequent steps, and the prediction of variability *in vitro* remains an unsettled topic of investigation. *In vitro* tests on variability should incorporate not just varying inhalation parameters (26), but also varying throat geometries (85) (and in some cases inhaler insertion angles (14)) to capture the large degree of variability observed between subjects, which complicates the experimental methods beyond the scope of the present work.

Conclusion

The combination of realistic *in vitro* experiment, lung deposition modeling, and pharmacokinetic modeling was shown to provide reasonable estimates of *in vivo* plasma concentration profiles of budesonide from DPIs. For the three DPIs examined here, significant differences *in vitro* resulted

in large differences in calculated regional lung deposition in the upper conducting (bronchial) airways and the alveolar region. However, deposition in the small conducting (bronchiolar) airways was comparatively modest for each DPI, despite the wide range of aerosol characteristics measured *in vitro*. Results here also suggest that for budesonide, peak systemic concentration is tied primarily to the alveolar dose, while the area under the curve is more dependent on the total lung dose. Tracheobronchial deposition was poorly correlated with pharmacokinetic data, suggesting that pharmacokinetic data for systemic exposure, by itself, may fail to provide useful information on deposition specifically in the conducting airways for budesonide, and likely for more dissolution-limited drugs as well. A strength of the proposed methodology lies in the ability to estimate commonly sought-after clinical parameters from *in vitro* data.

Acknowledgements

CAR gratefully acknowledges scholarship support from the Natural Sciences and Engineering Research Council (NSERC) of Canada, Alberta Innovates Technology Futures, and The Lung Association Alberta & NWT. AM and WF acknowledge funding from NSERC.

Conflicts of Interest

The authors declare that they have no conflict of interest.

References

1. Hossny E, Rosario N, Lee BW, Singh M, El-Ghoneimy D, Soh JY, et al. The use of inhaled corticosteroids in pediatric asthma: Update. World Allergy Organ J. 2016;9(1):1–24.

2. Chung KF, Wenzel SE, Brozek JL, Bush A, Castro M, Sterk PJ, et al. International ERS/ATS guidelines on definition, evaluation and treatment of severe asthma. Eur Respir

J. 2014;43(2):343–73.

3. Vogelmeier CF, Criner GJ, Martinez FJ, Anzueto A, Barnes PJ, Bourbeau J, et al. Global strategy for the diagnosis, management, and prevention of chronic obstructive lung disease 2017 report. Am J Respir Crit Care Med. 2017;195(5):557–82.

4. Pittas AG, Westcott GP, Balk EM. Efficacy, safety, and patient acceptability of Technosphere inhaled insulin for people with diabetes: A systematic review and meta-analysis. Lancet Diabetes Endocrinol. 2015;3(11):886–94.

5. San L, Estrada G, Oudovenko N, Montañés F, Dobrovolskaya N, Bukhanovskaya O, et al. PLACID study: A randomized trial comparing the efficacy and safety of inhaled loxapine versus intramuscular aripiprazole in acutely agitated patients with schizophrenia or bipolar disorder. Eur Neuropsychopharmacol. 2018;28(6):710–8.

6. Olanow CW, Stocchi F. Levodopa: A new look at an old friend. Mov Disord. 2018;33(6):859–66.

7. Martin AR, Moore CP, Finlay WH. Models of deposition, pharmacokinetics, and intersubject variability in respiratory drug delivery. Expert Opin Drug Deliv. 2018;15(12):1175–88.

8. Finlay WH. The mechanics of inhaled pharmaceutical aerosols : an introduction. 2nd ed. San Diego: Academic Press; 2019. 306 p.

9. Ruge CC, Kirch J, Lehr CM. Pulmonary drug delivery: From generating aerosols to overcoming biological barriers-therapeutic possibilities and technological challenges. Lancet Respir Med. 2013;1(5):402–13.

10. Loira-Pastoriza C, Todoroff J, Vanbever R. Delivery strategies for sustained drug release in

the lungs. Adv Drug Deliv Rev. 2014;75:81–91.

11. Koullapis P, Kassinos SC, Muela J, Perez-Segarra C, Rigola J, Lehmkuhl O, et al. Regional aerosol deposition in the human airways: The SimInhale benchmark case and a critical assessment of in silico methods. Eur J Pharm Sci. 2018;113(June 2017):77–94.

12. Walenga RL, Babiskin AH, Zhao L. In Silico Methods for Development of Generic Drug–Device Combination Orally Inhaled Drug Products. CPT Pharmacometrics Syst Pharmacol. 2019;8(6):359–70.

13. Wei W, Hindle M, Kaviratna A, Huynh B, Delvadia R, Sandell D, et al. In Vitro Tests for Aerosol Deposition . VI : Realistic Testing with Different Mouth – Throat Models and In Vitro — In Vivo Correlations for a Dry Powder. J Aerosol Med Pulm Drug Deliv. 2018;31(0):1–14.

14. Ruzycki CA, Martin AR, Finlay WH. An Exploration of Factors Affecting In Vitro Deposition of Pharmaceutical Aerosols in the Alberta Idealized Throat. J Aerosol Med Pulm Drug Deliv. 2019;32(6):405–17.

15. Bhagwat S, Schilling U, Chen MJ, Wei X, Delvadia R, Absar M, et al. Predicting Pulmonary Pharmacokinetics from In Vitro Properties of Dry Powder Inhalers. Pharm Res. 2017;34(12):2541–56.

16. Bäckman P, Tehler U, Olsson B. Predicting Exposure after Oral Inhalation of the Selective Glucocorticoid Receptor Modulator, AZD5423, Based on Dose, Deposition Pattern, and Mechanistic Modeling of Pulmonary Disposition. J Aerosol Med Pulm Drug Deliv. 2017;30(2):108–17.

17. Boger E, Fridén M. Physiologically Based Pharmacokinetic/Pharmacodynamic Modeling

Accurately Predicts the Better Bronchodilatory Effect of Inhaled Versus Oral Salbutamol Dosage Forms. J Aerosol Med Pulm Drug Deliv. 2019;32(1):1–12.

18. Caniga M, Cabal A, Mehta K, Ross DS, Gil MA, Woodhouse JD, et al. Preclinical Experimental and Mathematical Approaches for Assessing Effective Doses of Inhaled Drugs, Using Mometasone to Support Human Dose Predictions. J Aerosol Med Pulm Drug Deliv. 2016;29(4):362–77.

19. Martin AR, Finlay WH. Model Calculations of Regional Deposition and Disposition for Single Doses of Inhaled Liposomal and Dry Powder Ciprofloxacin. J Aerosol Med Pulm Drug Deliv. 2018;31(1):49–60.

20. Weber B, Hochhaus G. A Pharmacokinetic Simulation Tool for Inhaled Corticosteroids. Am Assoc Pharm Sci J. 2013;15(1):159–71.

21. Byron PR. Prediction of drug residence times in regions of the human respiratory tract following aerosol inhalation. J Pharm Sci. 1986;75(5):433–8.

22. Gonda I. Drugs Administered Directly into the Respiratory Tract: Modeling of the Duration. J Pharm Sci. 1988;77(4):340–6.

23. Soulele K, Macheras P, Karalis V. On the pharmacokinetics of two inhaled budesonide/formoterol combinations in asthma patients using modeling approaches. Pulm Pharmacol Ther. 2018;48(July 2017):168–78.

24. Lee SL, Saluja B, García-Arieta A, Santos GML, Li Y, Lu S, et al. Regulatory Considerations for Approval of Generic Inhalation Drug Products in the US, EU, Brazil, China, and India. AAPS J. 2015;17(5):1285–304.

25. Lu D, Lee SL, Lionberger RA, Choi S, Adams W, Caramenico HN, et al. International

Guidelines for Bioequivalence of Locally Acting Orally Inhaled Drug Products: Similarities and Differences. AAPS J. 2015;17(3):546–57.

26. Delvadia RR, Wei X, Longest PW, Venitz J, Byron PR. In Vitro Tests for Aerosol Deposition. IV: Simulating Variations in Human Breath Profiles for Realistic DPI Testing. J Aerosol Med Pulm Drug Deliv. 2016;29(2):196–206.

27. Weers J, Clark A. The Impact of Inspiratory Flow Rate on Drug Delivery to the Lungs with Dry Powder Inhalers. Pharm Res. 2017;34(3):507–28.

28. United States Pharmacopeia. USP 44(5) General Chapter <601> Inhalation and Nasal Drug Products - Aerosols, Sprays, and Powders - Performance Quality Tests. 2019.

29. United States Pharmacopeia. USP 45(2) Informative Chapter <1604> Data Interpretation of Aerodynamic Particle Size Distribution Measurements for Orally Inhaled Products. 2019.

30. Hinds WC. Aerosol technology : properties, behavior, and measurement of airborne particles. 2nd ed. Hoboken, NJ: Wiley; 1999.

31. Javaheri E, Shemirani FM, Pichelin M, Katz IM, Caillibotte G, Vehring R, et al. Deposition modeling of hygroscopic saline aerosols in the human respiratory tract : Comparison between air and helium – oxygen as carrier gases. J Aerosol Sci. 2013;64:81–93.

32. Finlay WH, Lange CF, King M, Speert DP. Lung Delivery of Aerosolized Dextran. 2000;161:91–7.

33. International Commission on Radiological Protection. Human respiratory tract model for radiological protection : a report of a task group of the International Commission on Radiological Protection. Vols. 24 1-3. Oxford, Eng. :Tarrytown, N.Y.: published for the International Commission on Radiological Protection by Pergamon; 1994. 482 p.

34. Chan TL, Lippmann M. Experimental measurements and empirical modelling of the regional deposition of inhaled particles in humans. Am Ind Hyg Assoc J. 1980;

35. Lange CF, Hancock REW, Samuel J, Finlay WH. In vitro aerosol delivery and regional airway surface liquid concentration of a liposomal cationic peptide. J Pharm Sci. 2001;90(10):1647–57.

36. May S, Jensen B, Weiler C, Wolkenhauer M, Schneider M, Lehr CM. Dissolution testing of powders for inhalation: Influence of particle deposition and modeling of dissolution profiles. Pharm Res. 2014;31(11):3211–24.

37. Ryrfeldt A, Andersson P, Edsbacker S, Tonnesson M, Davies D, Pauwels R. Pharmacokinetics and metabolism of budesonide, a selective glucocorticoid. Eur J Respir Dis. 1982;63(S 122):86–95.

38. Thorsson L, Edsbacker S, Conradson TB. Lung deposition of budesonide from Turbuhaler® is twice that from a pressurized metered-dose inhaler P-MDI. Eur Respir J. 1994;7(10):1839–44.

39. Hochhaus G, Möllmann H, Derendorf H, Gonzalez-Rothi RJ. Pharmacokinetic/pharmacodynamic aspects of aerosol therapy using glucocorticoids as a model. J Clin Pharmacol. 1997;37(10):881–92.

40. Yates JWT, Arundel PA. On the volume of distribution at steady state and its relationship with two-compartmental models. J Pharm Sci. 2008;97(1):111–22.

41. Dokoumetzidis A, Macheras P. A century of dissolution research: From Noyes and Whitney to the Biopharmaceutics Classification System. Int J Pharm. 2006;321(1–2):1–11.

42. Schürch S, Gehr P, Im Hof V, Geiser M, Green F. Surfactant displaces particles toward the

epithelium in airways and alveoli. Respir Physiol. 1990;80(1):17–32.

43. Hastedt JE, Bäckman P, Clark AR, Doub W, Hickey A, Hochhaus G, et al. Scope and relevance of a pulmonary biopharmaceutical classification system AAPS/FDA/USP Workshop March 16-17th, 2015 in Baltimore, MD. Am Assoc Pharm Sci Open. 2016;2(1):1.

44. Hintz RJ, Johnson KC. The effect of particle size distribution on dissolution rate and oral absorption. Int J Pharm. 1989;51(1):9–17.

45. Argenti D, Shah B, Heald D. A study comparing the clinical pharmacokinetics, pharmacodynamics, and tolerability of triamcinolone acetonide HFA-134a metered-dose inhaler and budesonide dry-powder inhaler following inhalation administration. J Clin Pharmacol. 2000;40(5):516–26.

46. Duddu SP, Sisk SA, Walter YH, Tarara TE, Trimble KR, Clark AR, et al. Improved lung delivery from a passive dry powder inhaler using an engineered PulmoSphere® powder. Pharm Res. 2002;19(5):689–95.

47. Harrison TW, Tattersfield AE. Plasma concentrations of fluticasone propionate and budesonide following inhalation from dry powder inhalers by healthy and asthmatic subjects. Thorax. 2003;58(3):258–60.

48. Lähelmä S, Kirjavainen M, Kela M, Herttuainen J, Vahteristo M, Silvasti M, et al. Equivalent lung deposition of budesonide in vivo: A comparison of dry powder inhalers using a pharmacokinetic method. Br J Clin Pharmacol. 2005;59(2):167–73.

49. Mollmann H, Wagner M, Krishnaswami S, Dimova H, Tang Y, Falcoz C, et al. Single-dose and steady-state pharmacokinetic and pharmacodynamic evaluation of therapeutically

clinically equivalent doses of inhaled fluticasone propionate and budesonide, given as diskus?? or turbohaler?? dry-powder inhalers to healthy subjects. J Clin Pharmacol. 2001;41(12):1329–38.

50. Thorsson L, Edsbacker S, Kallen A, Lofdahl C-G. Pharmacokinetics and systemic activity of fluticasone via Diskus and pMDI, and of budesonide via Turbuhaler. Br J Clin Pharmacol. 2001;52:529–38.

51. Mortimer KJ, Tattersfield AE, Tang Y, Wu K, Lewis S, Hochhaus G, et al. Plasma concentrations of fluticasone propionate and budesonide following inhalation: Effect of induced bronchoconstriction. Br J Clin Pharmacol. 2007;64(4):439–44.

52. Hämäläinen KM, Granander M, Toivanen P, Malinen A. Assessment of the systemic effects of budesonide inhaled from Easyhaler® and from Turbuhaler® in healthy male volunteers. Respir Med. 2001;95(11):863–9.

53. Mylan Products Ltd UK. Budelin Novolizer 200 micrograms per actuation inhalation powder [Internet]. 2018 [cited 2020 Jun 22]. Available from: https://www.medicines.org.uk/emc/product/9715/smpc

54. Meda Pharma GmbH. Budelin Novolizer 200 mikrogramov/odmerek prašek za inhaliranje [Internet]. 2017 [cited 2020 Jun 22]. Available from: http://www.cbz.si/cbz/bazazdr2.nsf/o/B0174ADF66EBFFE9C12579C2003F4EC8/$File/s-018681.pdf

55. Kaiser H, Aaronson D, Dockhorn R, Edsbäcker S, Korenblat P, Källén A. Dose-proportional pharmacokinetics of budesonide inhaled via Turbuhaler®. Br J Clin Pharmacol. 1999;48(3):309–16.

56. Parisini I, Cheng SJ, Symons DD, Murnane D. Potential of a cyclone prototype spacer to improve in vitro dry powder delivery. Pharm Res. 2014;31(5):1133–45.

57. Yoshida H, Kuwana A, Shibata H, Izutsu K, Goda Y. Comparison of Aerodynamic Particle Size Distribution Between a Next Generation Impactor and a Cascade Impactor at a Range of Flow Rates. AAPS PharmSciTech. 2017;18(3):646–53.

58. Wei X, Hindle M, Delvadia RR, Byron PR. In Vitro Tests for Aerosol Deposition. V: Using Realistic Testing to Estimate Variations in Aerosol Properties at the Trachea. J Aerosol Med Pulm Drug Deliv. 2017;30(5):jamp.2016.1349.

59. Dehaan WH, Finlay WH. Predicting extrathoracic deposition from dry powder inhalers. J Aerosol Sci. 2004;35:309–31.

60. Grgic B, Finlay WH, Burnell PKP, Heenan AF. In vitro intersubject and intrasubject deposition measurements in realistic mouth – throat geometries. J Aerosol Sci. 2004;35:1025–40.

61. Walenga RL, Longest PW. Current Inhalers Deliver Very Small Doses to the Lower Tracheobronchial Airways: Assessment of Healthy and Constricted Lungs. J Pharm Sci. 2016;105(1):147–59.

62. Hamid Q, Song Y, Kotsimbos TC, Minshall E, Bai TR, Hegele RG, et al. Inflammation of small airways in asthma. J Allergy Clin Immunol. 1997;100(1):44–51.

63. N. Richard Dekhuijzen P. Anti-Inflammatory Drug Targeting in Asthma. Should Inhaled Corticosteroids Reach the Small Airways? Curr Drug ther. 2013;7(4):248–54.

64. Van Den Berge M, Ten Hacken NHT, Van Der Wiel E, Postma DS. Treatment of the bronchial tree from beginning to end: Targeting small airway inflammation in asthma.

Allergy Eur J Allergy Clin Immunol. 2013;68(1):16–26.

65. Ostrovski Y, Dorfman S, Mezhericher M, Kassinos S, Sznitman J. Targeted Drug Delivery to Upper Airways Using a Pulsed Aerosol Bolus and Inhaled Volume Tracking Method. Flow, Turbul Combust. 2019;102(1):73–87.

66. Tian G, Longest PW, Su G, Hindle M. Characterization of respiratory drug delivery with enhanced condensational growth using an individual path model of the entire tracheobronchial airways. Ann Biomed Eng. 2011;39(3):1136–53.

67. Kopsch T, Murnane D, Symons D. Optimizing the Entrainment Geometry of a Dry Powder Inhaler: Methodology and Preliminary Results. Pharm Res. 2016;33(11):2668–79.

68. Borgstrom L, Bondesson E, Moren F, Trofast E, Newman SP. Lung deposition of budesonide inhaled via Turbuhaler®: A comparison with terbutaline sulphate in normal subjects. Eur Respir J. 1994;7(1):69–73.

69. Newman SP, Pitcairn GR, Hirst PH, Bacon RE, O'Keefe E, Reiners M, et al. Scintigraphic comparison of budesonide deposition from two dry powder inhalers. Eur Respir J. 2000;16(1):178–83.

70. Hirst PH, Bacon RE, Pitcairn GR, Silvasti M, Newman SP. A comparison of the lung deposition of budesonide from Easyhlaler®, Turbuhaler® and pMDI plus spacer in asthmatic patients. Respir Med. 2001;95(9):720–7.

71. Hirst PH, Newman SP, Clark DA, Hertog MGL. Lung deposition of budesonide from the novel dry powder inhaler Airmax™. Respir Med. 2002;96(6):389–96.

72. Fleming J, Conway J, Majoral C, Katz I, Caillibotte G, Pichelin M, et al. Controlled, parametric, individualized, 2-D and 3-D imaging measurements of aerosol deposition in the

respiratory tract of asthmatic human subjects for model validation. J Aerosol Med Pulm Drug Deliv. 2015;28(6):432–51.

73. Smith DJ, Gaffney EA, Blake JR. Modelling mucociliary clearance. Respir Physiol Neurobiol. 2008;163(1–3):178–88.

74. Eriksson J, Thörn H, Sjögren E, Holmstén L, Rubin K, Lennernäs H. Pulmonary Dissolution of Poorly Soluble Compounds Studied in an ex Vivo Rat Lung Model. Mol Pharm. 2019;16:3053–64.

75. Bäckman P, Olsson B. Pulmonary Drug Dissolution, Regional Retention and Systemic Absorption: Understanding their Interactions Through Mechanistic Modeling. Respir Drug Deliv 2020. 2020;50:113–22.

76. Floroiu A, Klein M, Krämer J, Lehr CM. Towards standardized dissolution techniques for in vitro performance testing of dry powder inhalers. Dissolution Technol. 2018;25(3):6–18.

77. Hochhaus G, Chen M, Shur J, Kurumaddali A, Schilling U, Jiao Y, et al. Unraveling the Pulmonary Fate of Fluticasone and Friends : Meeting the Physiologic and Pharmacokinetic Challenges. Respir Drug Deliv 2020. 2020;139–46.

78. Bäckman P, Arora S, Couet W, Forbes B, de Kruijf W, Paudel A. Advances in experimental and mechanistic computational models to understand pulmonary exposure to inhaled drugs. Eur J Pharm Sci. 2018;113(June 2017):41–52.

79. Olsson B, Borgström L, Lundbäck H, Svensson M. Validation of a General In Vitro Approach for Prediction of Total Lung Deposition in Healthy Adults for Pharmaceutical Inhalation Products . J Aerosol Med Pulm Drug Deliv. 2013;26(6):355–69.

80. Chuchalin AG, Kremer H-J, Metzenauer P, O'Keefe E, Hermann R. Clinical equivalence

trial on budesonide delivered either by the Novolizer® multidose dry powder inhaler or the Turbuhaler® in asthmatic patients. Respiration. 2002;69(6):502–8.

81. Vanto T, Hämäläinen KM, Vahteristo M, Wille S, Njå F, Hyldebrandt N. Comparison of Two Budesonide Dry Powder Inhalers in the Treatment of Asthma in Children. J Aerosol Med Depos Clear Eff Lung. 2004;17(1):15–24.

82. Schweisfurth H, Malinen A, Koskela T, Toivanen P, Ranki-Pesonen M. Comparison of two budesonide powder inhalers, Easyhaler® and Turbuhaler®, in steroid-naïve asthmatic patients. Respir Med. 2002;96(8):599–606.

83. Van Den Brink KIM, Boorsma M, Staal-Van Den Brekel AJ, Edsbäcker S, Wouters EF, Thorsson L. Evidence of the in vivo esterification of budesonide in human airways. Br J Clin Pharmacol. 2008;66(1):27–35.

84. Shao J, Talton J, Wang Y, Winner L, Hochhaus G. Quantitative Assessment of Pulmonary Targeting of Inhaled Corticosteroids Using Ex Vivo Receptor Binding Studies. AAPS J. 2020;22(2):1–10.

85. Ruzycki CA, Yang M, Chan H-K, Finlay WH. Improved prediction of intersubject variability in extrathoracic aerosol deposition using algebraic correlations. Aerosol Sci Technol. 2017;51(6):667–73.

Appendix A – Volumetric Flowrates

The Delvadia et al semi-idealized inhalation profiles are presented in terms of the volumetric flowrate exiting the inhaler mouthpiece. The setup in Figure 1 can provide an indirect measure of this flowrate by considering a mass balance of flow. Consider a control volume encompassing the supply line, the breathing machine line, the vacuum line downstream of the NGI, and the airflow entering the DPI. The equation for conservation of mass in this control volume is:

$$\frac{dm}{dt} = \sum \dot{m}_{\text{in}} - \sum \dot{m}_{\text{out}} \qquad \text{A - 1}$$

The time rate of change of mass inside the control volume, dm/dt, is considered negligible relative to the magnitudes of the inlet and outlet flows. This assumption is justified by noting that all flows here have Mach numbers less than 0.3 (i.e. flow can be considered incompressible, so changes in density are small) and the walls of the control volume are rigid (i.e. the actual volume of gas contained in the control volume remains constant). Noting that $m = \rho V$ (mass equals density times volume), expanding with the product rule for differentiation, and using the above physical reasoning (incompressible flow and a rigid control volume), dm/dt is:

$$\frac{dm}{dt} = \frac{d(\rho V)}{dt} = \rho \frac{dV}{dt} + Q \frac{d\rho}{dt} = 0 \qquad \text{A - 2}$$

The equation for conservation of mass becomes, after expressing the inlet and outlet flows in terms of their volumetric flowrates $Q_{\text{vol,supply}}$, $Q_{\text{vol,HBM}}$, $Q_{\text{vol,vacuum}}$, and $Q_{\text{vol,DPI}}$:

$$\rho_{\text{supply}} Q_{\text{vol,supply}} + \rho_{\text{DPI}} Q_{\text{vol,DPI}} = \rho_{\text{HBM}} Q_{\text{vol,HBM}} + \rho_{\text{vacuum}} Q_{\text{vol,vacuum}} \qquad \text{A - 3}$$

Equation A - 3 can be recast in terms of standard flowrates using the ideal gas law as follows. The volumetric flowrate at a particular temperature and pressure relates to the standard flowrate as:

$$Q_{\mathrm{vol,m}}(t) = Q_{\mathrm{std,m}}(t)\frac{P_{\mathrm{ref}}}{T_{\mathrm{ref}}}\frac{T_{\mathrm{m}}}{P_{\mathrm{m}}} \qquad \text{A - 4}$$

From the ideal gas law:

$$\rho_{\mathrm{m}} = \frac{P_{\mathrm{m}}}{R_{\mathrm{specific}}T_{\mathrm{m}}} \qquad \text{A - 5}$$

Equation A - 4 can then be expressed as:

$$\rho_{\mathrm{m}}Q_{\mathrm{vol,m}}(t) = \rho_{\mathrm{ref}}Q_{\mathrm{std,m}}(t) \qquad \text{A - 6}$$

Here ρ_{m} is the air density at which the volumetric flowrate is desired (dependent on temperature and pressure), while ρ_{ref} is a reference density (equal to approximately 1.2 kg/m^3 for TSI calibrated flowmeters). With suitable substitutions, Equation A - 3 takes a simple form as all density terms become ρ_{ref}. Further rearranging to solve for the unmeasured flowrate entering the DPI, Equation A - 3 becomes:

$$Q_{\mathrm{std,DPI}}(t) = Q_{\mathrm{std,HBM}}(t) + Q_{\mathrm{std,vacuum}}(t) - Q_{\mathrm{std,supply}}(t) \qquad \text{A - 7}$$

Flowrates on the right hand side of Equation A - 7 are known, allowing for the straightforward calculation of the standard flowrate generated through the DPI, $Q_{\mathrm{std,DPI}}$. Calculation of the volumetric flowrate exiting the DPI mouthpiece can then be performed using A - 8 (Ruzycki et al, J Aerosol Med Pulm Drug Deliv 2019;32(6):405-417).

$$Q_{\mathrm{vol,DPI\ exit}}(t) = Q_{\mathrm{std,DPI}}(t)\frac{T_{\mathrm{m}}}{T_{\mathrm{ref}}}\frac{P_{\mathrm{ref}}}{\left(P_{\mathrm{m}} - \left[RQ_{\mathrm{std,DPI}}(t)\frac{T_{\mathrm{m}}}{T_{\mathrm{ref}}}\frac{P_{\mathrm{ref}}}{P_{\mathrm{m}}}\right]^2\right)} \qquad \text{A - 8}$$

P_{ref} equals 101.3 kPa, T_{ref} equals 21.11°C (294.26 K), and R is the device resistance (taken as the reference value measured at sea level). Equation A - 8 assumes that the effect of ambient pressure on inhaler resistance is negligible (reasonable for moderate altitudes; Titosky et al, J Pharm Sci 2014;103:2116-2124; Ruzycki et al, J Aerosol Med Pulm Drug Deliv 2018;31(4):221-236). Furthermore, the derivation assumes that the relation between pressure drop and flowrate is quasi-steady, a reasonable assumption given the small volume of the inhaler relative to the inhalation flowrate.

Appendix B – Equations Describing the Pharmacokinetic Model

The equations describing the pharmacokinetic model shown schematically in Figure 2 of the main text are summarized in this Appendix. Note that initial deposited masses in each generation of the tracheobronchial airways and in the alveolar region (F_{i}, $0 \leq \mathrm{i} \leq 14$, and F_{ALV}, respectively) come directly from the regional deposition model discussed in the main text, while the initial dose in the gastrointestinal tract is taken as the dose measured in the Alberta Idealized Throat *in vitro*. Rate constants describing mucociliary clearance ($k_{\mathrm{muc,i}}$) and the volume of the airway surface liquid in each generation $V_{\mathrm{ASL,i}}$ come from the airway surface liquid model discussed in the main text. Values for other rate constants and critical parameters are provided in the main text with references to the literature.

Gastrointestinal tract compartment drug mass, m_{A}:

$$\frac{dm_{\mathrm{A}}}{dt} = -k_{\mathrm{a}} m_{\mathrm{A}} + k_{\mathrm{muc},0}(m_{0,1} + m_{0,2}) \qquad \text{B - 1}$$

Equation B - 1 is subject to the initial condition m_{A} equal to the dose measured in the Alberta Idealized Throat at time $t = 0$.

Central compartment drug mass, m_{X}:

$$\frac{dm_{\mathrm{X}}}{dt} = -(k_{12} + k_{01}) m_{\mathrm{X}} + F_{\mathrm{BA}} k_{\mathrm{a}} m_{\mathrm{A}} + k_{21} m_{\mathrm{P}} + k_{\mathrm{ALV}} m_{\mathrm{ALV},2} + k_{\mathrm{TB}} \sum_{i=0}^{14} m_{i,2} \qquad \text{B - 2}$$

Equation B - 2 is subject to the initial condition $m_{\mathrm{X}} = 0$ at time $t = 0$.

Central compartment drug concentration, c_{X}:

$$c_{\mathrm{X}} = \frac{m_{\mathrm{X}}}{V_{\mathrm{C}}} \qquad \text{B - 3}$$

Where the volume of distribution, V_{C}, was calculated via Equation 3 as discussed in the main text.

Peripheral compartment drug mass, m_{P}:

$$\frac{dm_{\mathrm{P}}}{dt} = k_{12}m_{\mathrm{X}} - k_{21}m_{\mathrm{P}} \qquad \text{B - 4}$$

Equation B - 4 is subject to the initial condition $m_{\mathrm{P}} = 0$ at time $t = 0$.

i$^{\mathrm{th}}$ tracheobronchial airway compartment drug mass, m_{i} ($0 \leq i < 14$):

$$\frac{dm_{\mathrm{i,1}}}{dt} = -K_{\mathrm{diss,TB}}m_{\mathrm{i,1}}(c_{\mathrm{S}} - c_{\mathrm{i}}) - k_{\mathrm{muc,i}}m_{\mathrm{i,1}} + k_{\mathrm{muc,i+1}}m_{\mathrm{i+1,1}} \qquad \text{B - 5}$$

$$\frac{dm_{\mathrm{i,2}}}{dt} = K_{\mathrm{diss,TB}}m_{\mathrm{i,1}}(c_{\mathrm{S}} - c_{\mathrm{i}}) - k_{\mathrm{muc,i}}m_{\mathrm{i,2}} + k_{\mathrm{muc,i+1}}m_{\mathrm{i+1,2}} - k_{\mathrm{TB}}m_{\mathrm{i,2}} \qquad \text{B - 6}$$

i$^{\mathrm{th}}$ tracheobronchial airway compartment drug mass, m_{i} ($i = 14$):

$$\frac{dm_{\mathrm{i,1}}}{dt} = -K_{\mathrm{diss,TB}}m_{\mathrm{i,1}}(c_{\mathrm{S}} - c_{\mathrm{i}}) - k_{\mathrm{muc,i}}m_{\mathrm{i,1}} \qquad \text{B - 7}$$

$$\frac{dm_{\mathrm{i,2}}}{dt} = K_{\mathrm{diss,TB}}m_{\mathrm{i,1}}(c_{\mathrm{S}} - c_{\mathrm{i}}) - k_{\mathrm{muc,i}}m_{\mathrm{i,2}} - k_{\mathrm{TB}}m_{\mathrm{i,2}} \qquad \text{B - 8}$$

i$^{\mathrm{th}}$ tracheobronchial airway compartment drug concentration, c_{i} ($0 \leq i \leq 14$):

$$c_{\mathrm{i}} = \frac{m_{\mathrm{i,2}}}{V_{\mathrm{ASL,i}}} \qquad \text{B - 9}$$

Alveolar compartment drug mass, m_{ALV}:

$$\frac{dm_{\mathrm{ALV},1}}{dt} = -k_{\mathrm{diss,ALV}} m_{\mathrm{ALV},1} \qquad \text{B - 10}$$

$$\frac{dm_{\mathrm{ALV},2}}{dt} = k_{\mathrm{diss,ALV}} m_{\mathrm{ALV},1} - k_{\mathrm{ALV}} m_{\mathrm{ALV},2} \qquad \text{B - 11}$$

Equation B – 5, B – 7, and B – 10 are subject to the initial condition $m_{\mathrm{i},1} = F_{\mathrm{i}}$ at time $t = 0$.

Equation B – 6, B – 8, and B – 11 are subject to the initial condition $m_{\mathrm{i},2} = 0$ at time $t = 0$.